

Milestone Report

Hierarchical Calibration and Validation of High-fidelity CFD Models with C2U Experiments

Work Performed Under

PNNL -60174
LANL -FE-101-002-FY10
NETL -RES-0004000.6.600.007.002

Prepared by
Pacific Northwest National Laboratory
Richland, Washington 99352

In collaboration with Los Alamos National Laboratory, the National Energy Technology Laboratory

Prepared for the
U.S. Department of Energy
National Energy Technology Laboratory

31 March 2014



Revision Log

Revision	Date	Revised By:	Description
0.1	March 15, 2014	Kevin Lai	Original draft
0.2	March 21, 2014	Wenxiao Pan	Sections added
0.3	March 28, 2014	Zhijie Xu	Sections added
0.4	April 2, 2014	Curtis Storlie	Sections added
0.5	April 10, 2014	Xin Sun	Proof reading
0.6	April 26, 2014	Tingwen Li	Proof reading
0.7	April 28, 2014	Jean Dietiker	Proof reading
0.8	April 29, 2014	Larry Shadle	Proof reading
1.0	May 2, 2014	Xin Sun	Final Version

Disclaimer

This report was prepared as an account of work sponsored by an agency of the United States Government. Neither the United States Government nor any agency thereof, nor any of their employees, makes any warranty, express or implied, or assumes any legal liability or responsibility for the accuracy, completeness, or usefulness of any information, apparatus, product, or process disclosed, or represents that its use would not infringe privately owned rights. Reference herein to any specific commercial product, process, or service by trade name, trademark, manufacturer, or otherwise does not necessarily constitute or imply its endorsement, recommendation, or favoring by the United States Government or any agency thereof. The views and opinions of authors expressed herein do not necessarily state or reflect those of the United States Government or any agency thereof.

Acknowledgement of Funding

This project was funded under the Carbon Capture Simulation Initiative under the following FWP's and contracts:

LANL - FE-101-002-FY10
PNNL - 60174
LLNL - FEW0180
LBNL - CSNW1130
NETL - RES-0004000.6.600.007.002

Table of Content

1. INTRODUCTION	5
2. GENERAL DESCRIPTION OF MODEL CALIBRATION AND UQ.....	6
3. MODELING THE CARBON CAPTURE UNIT (C2U)	7
3.1 Experiment Design and Operating Conditions for Solid Sorbent Carbon Capture System (C2U)	7
3.3 MFIX CFD Model Development.....	9
4. AX COLD FLOW	11
4.1 CFD Simulation Results for AX Cold Flow	11
4.2 UQ analysis and results for AX Cold Flow.....	12
5. 32D COLD FLOW.....	16
5.1 CFD Simulation Results for 32D Cold Flow	16
5.2 UQ Analysis and Results for 32D Cold Flow.....	17
6. 32D HOT NON-REACTING FLOW.....	19
6.1 CFD Simulation Results for 32D Hot Non-Reacting Flow	19
6.2 UQ Analysis and Results for 32D Hot Non-Reacting Flow.....	20
7. 32D REACTING FLOW	23
7.1 CFD Simulation Results for 32D Reacting Flow.....	23
7.2 UQ Analysis and Results for 32D Reacting Flow	32

List of Figures

Figure 1: CCSI Hierarchical CFD Validation	6
Figure 2: Schematic plot of experiment setup and locations of various sensors.....	8
Figure 3 Illustration of MFIX CFD Model	9
Figure 4 Snapshots of void fraction and pressure distribution for AX cold flow	12
Figure 5 Snapshots of solids density distribution and the calculated pressure drop along the reactor height	12
Figure 6 Validation of AX cold flow PDT3820 pressure drop.....	13
Figure 7 Marginal posterior distributions of the five model parameters (provided as histograms of the MCMC sample) along with the assumed prior distributions (blue curves)	14
Figure 8 Marginal posterior distributions of the six model parameters (now including effective particle size) for the AX cold flow unit problem.	15
Figure 9 Experimental pressure drop data at PDT3820 across flow rate, along with posterior emulator results and emulator plus discrepancy results for model without particle size calibrated (left pane) and model with particle size included in the calibration (right pane). The light colored lines are posterior realizations, while the thick line is the posterior mean curve. Black vertical lines are error bars for the steady state mean pressure drop for each experimental data point.	16
Figure 10 Sorbent 32D particle size distribution	17
Figure 11 Marginal posterior distributions of the five model parameters resulting from the 32D cold flow unit problem (provided as histograms of the MCMC sample) along with the assumed prior distributions (blue curves).....	18
Figure 12 Experimental pressure drop data at location PDT3820 across gas flow rate, along with posterior emulator results and emulator plus discrepancy results. The light colored lines are posterior realizations, while the thick lines are posterior mean curves. Black vertical lines are error bars for the steady state mean pressure drop for each experimental data point.	18
Figure 13 32D Hot Non-Reacting Flow Validations.....	19
Figure 14 Time-varying boundary conditions.....	20
Figure 15 Bed temperature vs. time	20
Figure 16 Marginal posterior distributions of the six model parameters for MFIX, including particle size, resulting from the 32D hot/non-reacting flow calibration.	21
Figure 17 Fitted plots for pressure drop at location PDT3820 . Blue is model prediction, red is model plus a model discrepancy correction. The model predicts the data relatively well as the model discrepancy is not prominent here.	22
Figure 18 Fitted plots for pressure drop at location PDT3860 . Blue is model prediction, red is model plus a model discrepancy correction. The model predicts the data relatively well as the model discrepancy is not prominent here.	23
Figure 19 CO ₂ adsorption curve for run #2.....	26
Figure 20 Distribution of experiment parameters	27
Figure 21 Experiment data shows decrease in CO ₂ adsorption capacity over time	28
Figure 22 Average pressured drop (PDT3820) for 67 runs.....	29
Figure 23 Average bed temperature for all 67 cases	29
Figure 24 Normalized CO ₂ adsorption for all 67 cases, and comparison with experiment data.....	30
Figure 25 CO ₂ adsorption breakthrough curve	30

Figure 26 Time for C2U unit to adsorb 25% and 50% of total capacity	31
Figure 27 Time for C2U unit to adsorb 75% total capacity	31
Figure 28 Experiment CO ₂ adsorption time Vs. simulated adsorption time for 25%, 50% and 75% adsorption.....	32
Figure 29 Functional decompositions for three of the experimental runs (top row) and three simulator runs at corresponding experimental input settings and the parameter settings used in Section 7.1.....	33
Figure 30 Pairwise scatter plots of the space filling experimental design for C2U runs for adsorption. Replicated conditions are plotted in red.....	35
Figure 31Histograms of the marginal posterior distributions of the 15 model parameters. Prior density is given by the blue curve. The set points for the 71 MFIX validation runs described in Section 7.1 are given as the red ticks for reference.....	36
Figure 32 Bivariate view of the posterior distribution for all pairwise combinations of the seven influential model parameters. The univariate posterior distribution for a given parameter is provided along the diagonal.....	37
Figure 33 Predictions of the breakthrough curves for the nine held out runs along with experimental data (grey points) and experimental error bands based on the functional decomposition (green).....	39
Figure 34 Emulator model predictions versus the observed data for the coefficients of the breakthrough curve decomposition along with predictions versus observed for the PDT3820 pressure drop.....	40

List of Tables

Table 1 Parameters for 32D Kinetics	24
Table 2 Experimental Inputs	34
Table 3 Model Parameters and prior distributions	34

Milestone Report on the Hierarchical Calibration and Validation of High-fidelity CFD Models with C2U Experiments

Kevin Lai, Zhijie Xu, Wenzhao Pan, Lawrence Shadle, Curtis Storlie, Jeff Dietiker,
Tingwen Li, Sebastien Darteville, Xin Sun

1. Introduction

Over the past several decades, there has been increasing concerns over the effects of anthropogenic emissions of greenhouse gases on the global climate change. Post-combustion carbon capture and subsequent sequestration are being considered as a potential route in reducing the carbon dioxide emission from coal-fired power plants, which contributes to roughly 80% of the greenhouse gas. The Carbon Capture Simulation Initiative (CCSI), a partnership among DOE national laboratories, industry, and universities, is developing state-of-the-art computational modeling and simulation tools aimed at dramatically accelerating the development and deployment of post-combustion carbon capture technologies. As a candidate for large scale post-combustion CO₂ capture, solid sorbent-based capture system is attracting researchers' attention with the potential to reduce energy consumption, improve regeneration, enable greater capacity, and offer selectivity as well as ease of handling. In CCSI, high fidelity computational fluid dynamics (CFD) simulations are used to simulate the device-scale complex multiphase reactive flow phenomena to evaluate the specific reactor design and to provide device-scale reduced order models for plant-level system synthesis simulations. To achieve the ultimate modeling and simulation goal of quantifying predictive confidence, a hierarchical validation methodology has been developed and implemented, from basic unit problems, up-scaling with filtering models, to C2U batch, eventually to large scale systems; and from simple to more complexity, the modeling validation starts with cold flow, adding heat transfer, and adding chemical reactions to the multi-physics simulations in that order.

According to this hierarchical validation approach, a series of validation experiments and corresponding simulation runs have been performed as shown in Figure 1 with unit problems of increasing levels of complexity. First is the cold and non-reacting flow with sorbent AX as the solid phase; then cold flow with a different sorbent 32D; next, a hot but non-reacting flow with 32D sorbent; and finally reacting flow with 32D. It is in this order that we started our validation process with multiphase flow hydrodynamics only validation, adding heat transport, and finally modeling chemical reactions in our multi-phase flow validations.

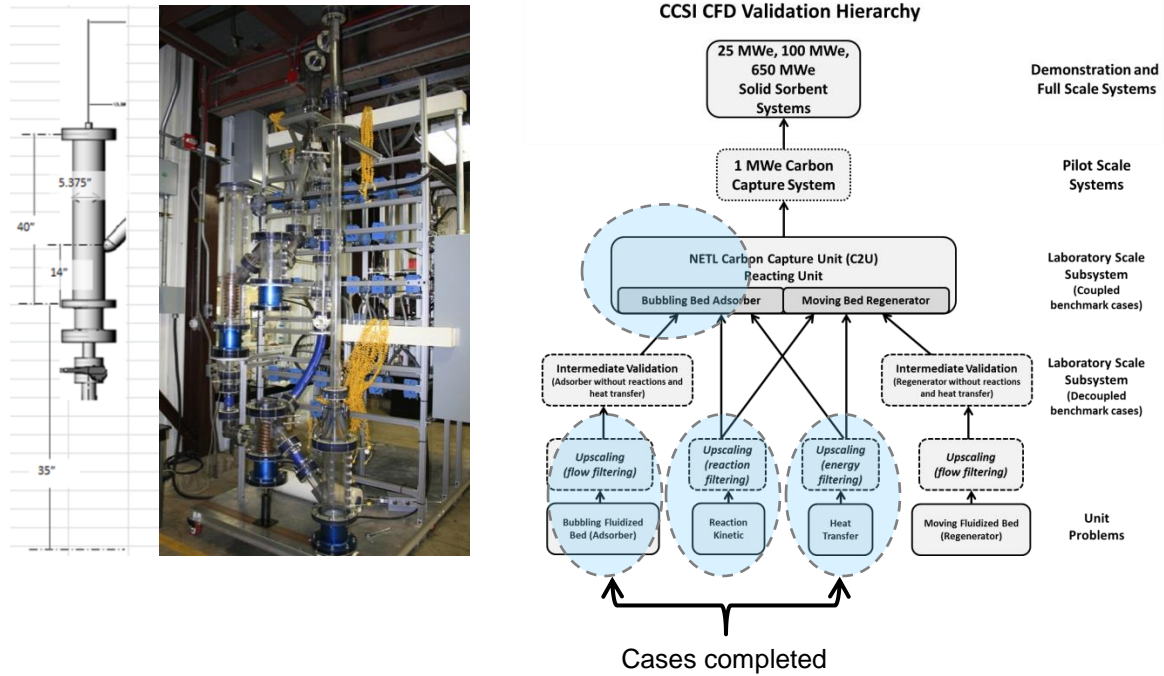


Figure 1: CCSI Hierarchical CFD Validation

Compared with our previous Milestone Report (April 2013) where only the CFD hydrodynamics validation was made, this report covers the validation on all three aspects of this complex multi-physics multi-phase reactive flow problem. Based on the simulation results with the unit problems, we are able to provide the calibrated model parameters and discrepancy functions between the model prediction and experiment observation. In Task 4, we have developed: 1) CFD models for bubbling bed adsorber of Carbon Capture Unit (C2U) system; 2) Adaptive sampling capability for UQ. 3) Model validation for C2U and Bayesian calibration for CFD models.

2. General Description of Model Calibration and UQ

The computational MFIX model was analyzed with the same statistical uncertainty quantification techniques as those used in the bubbling bed unit problem (Lane et.al 2013), including sensitivity analysis (Saltelli 2000, Storlie et.al 2009), Bayesian calibration and model assessment (Kennedy et.al 2001, Higdon et.al 2004, Storlie et.al. 2013). These tools were used to evaluate the model and determine the optimal input parameters.

Analysis begins by identifying model parameters $\Theta = [\theta_1, \dots, \theta_p]$, that are thought to be significant and have an associated uncertainty in their values. The relevant parameters identified in each C2U problem are described in their respective sections.

The BSS-ANOVA calibration routine used for analysis in what follows is described in detail in Storlie et.al. 2013, while a brief overview is also provided in Lane et.al 2013. Essentially the approach builds upon the approaches of Kennedy et.al 2001 and Higdon et.al 2004, by first placing a prior probability distribution on the value of the unknown model parameters. This prior distribution is then updated by conditioning on the experimental data

and the CFD model runs to produce a posterior distribution of plausible values for the model parameters. The procedure requires that the CFD code be evaluated at a sample of parameter values, then inherently makes use of an *emulator* (i.e., statistical response surface model) to evaluate the CFD model (at locations that it has yet to be run) as needed in the MCMC estimation algorithm. It is important to understand that the emulator is not simply a fast surrogate model for the CFD code, it accounts for the additional uncertainty inherent in the estimation of a response surface. There is also a discrepancy function that is estimated along with the model parameters and the emulator that accounts for the possible gap between experimental observations and the model results. This discrepancy function can then be studied to perform a model assessment (i.e., “validate” the model). Please refer to Storlie et.al. 2013 for further details.

3. Modeling the Carbon Capture Unit (C2U)

This section of the report presents the CFD analysis framework for the multiphase flow of sorbent particles and the gas phases in the carbon capture unit (C2U) at NETL. The aims of this work are: (i) to demonstrate the modeling capabilities for C2U, (ii) to validate and calibrate the CFD model parameters with C2U data at unit problem level, and (iii) to identify the discrepancy function between the model prediction and the observation. The information and knowledge obtained from these simulations will be used to predict the carbon capture performance for the device-scale 1MW system.

3.1 Experiment Design and Operating Conditions for Solid Sorbent Carbon Capture System (C2U)

A picture of the C2U experimental facility at NETL is shown on the left-hand side of Figure 1. The schematics in Figure 2 show various sensors that control and measure flow, pressure, and temperature during operation.

The characteristic dimensions of the reactor cylinder include the radius 0.0685 m and height of 1.003 m. Two sets of spiral cooling coils with the height of about 0.31 m are placed at the lower part of the reactor. Cooling or heating oil is circulating in the coil to achieve a desired bed temperature. Inside the C2U unit, a specific amount of sorbent particles, either 3.1 kg of AX or 1.62kg of 32D, is placed. Synthetic flue gas with specific flow rate, composition, and temperature is blown from the bottom of the unit by a flow transmitter controller (FTC). The gas exits at the top via a tube with 1-inch diameter.

For the cold flow experiments with 3.1kg sorbent AX, the inlet gas consists of mainly nitrogen N₂ with a very small amount of moisture (H₂O). Without CO₂, there is no reaction and no heat is generated. Coil is not filled with heating or cooling oil. The main quantity of interest (QOI) in this set of experiments has been the pressure drop measured by the pressure transducer PDT3820 in the fluidized bed.

For the 32D cold flow experiments, all conditions remain the same as those for AX cold flow except that a different solid mass of sorbents, i.e., 1.62 kg of 32D sorbent is used in the C2U unit. The QOIs measured in this set of experiments is also the pressure drop.

In the 32D hot but non-reacting flow, the inlet gas temperature is varied and so is the coil temperature by circulating oil with a specific temperature in the coils. The inlet gas is the same N₂ nitrogen without CO₂. The QOIs measured in this set of experiments include pressure drop as well as bed temperature.

Finally the experiments of 32D reacting flow involve the most comprehensive multi-physics mechanisms including hydrodynamics, heat transfer, and chemical reactions. Synthetic flue gas with carefully designed CO₂ concentration is used as the inlet gas, and the coil temperature is maintained by the temperature of flowing oil to achieve the desired bed temperature in the C2U unit. In addition to pressure drop and bed temperature, the QOIs measured in this round of the experiments also include CO₂ concentration at exit with which the CO₂ adsorption capacity and the breakthrough curve can be calculated.

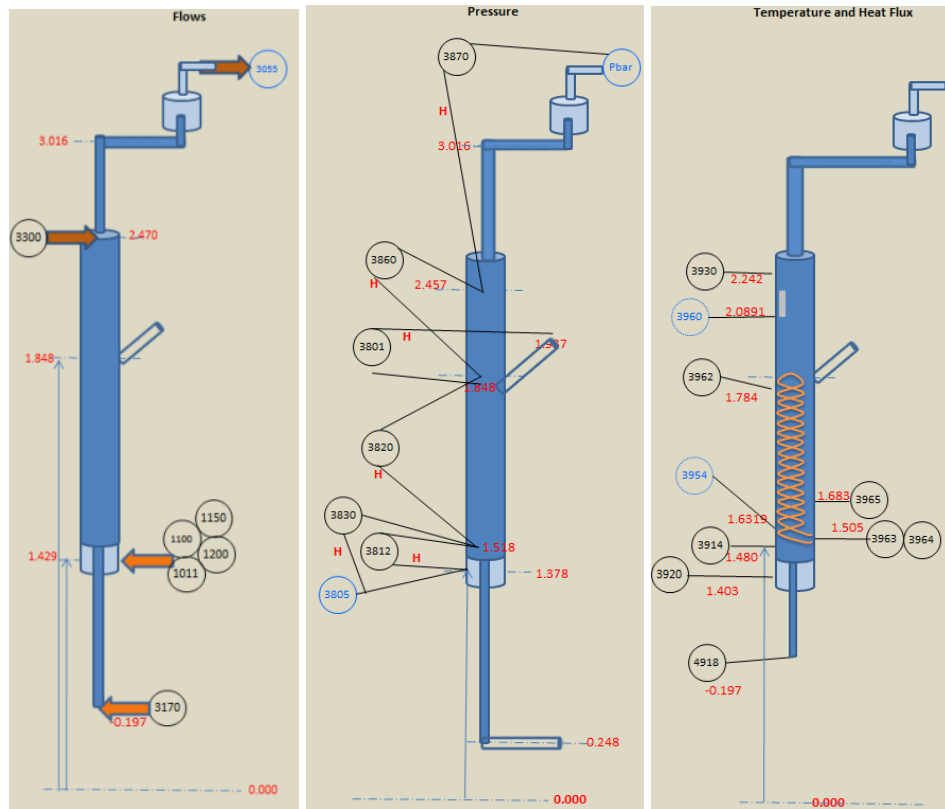


Figure 2: Schematic plot of experiment setup and locations of various sensors

3.3 MFIX CFD Model Development

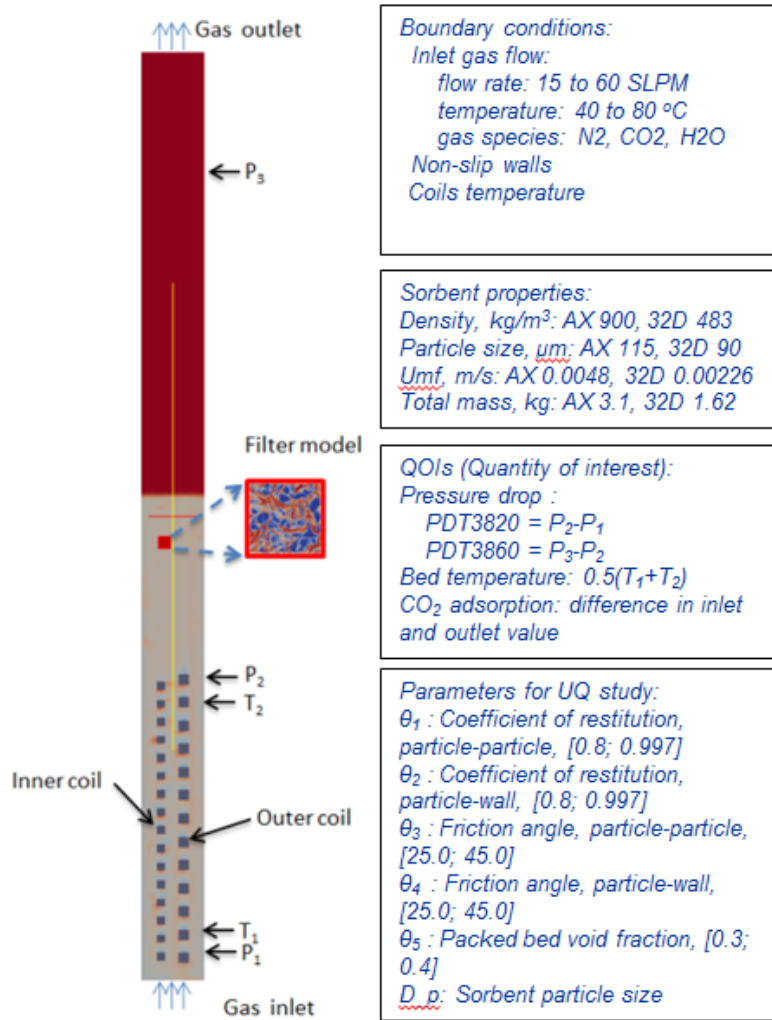


Figure 3 Illustration of MFIX CFD Model

A 2D axi-symmetric CFD model is developed to simulate the multi-phase gas particle flow (with and without reactions) in C2U, see Figure 3. Filtered subgrid models (Igci et al., 2008; Igci and Sundaresan, 2011; Milioli et al., 2013) were employed here to effectively incorporate the effects of flow heterogeneity of the solid particle structures in a coarse grid simulation as such.

The boundary conditions used for the system are also shown in Figure 3. The gas inlet on the bottom is modeled as a mass inflow (MI) boundary. The outlet at the top is of 1-inch diameter for gas only to exit. The inlet mass flow rate for the fluidizing gas, as well as the gas composition are varying in the experiments and thus in the simulations. To prevent sorbents from escaping the computational domain, semi-permeable boundaries are applied on both the bottom and the top. Two coils are explicitly modeled as internal structures with no-slip boundary conditions for the flow. For simulations involving heat transfer, the temperature at the coil boundary conditions is set to the average coil temperature.

The solids are either AX or 32D, both are amine-based sorbent, with specified quantity. The total mass is of 3.1 kg for AX sorbent and 1.62 kg for 32D sorbent. The solid was designed to remain in the C2U unit throughout the entire experiment cycles, although some small elutriation has been observed over the duration of 32D adsorption and regenerating cycles. The small amount of elutriation is not modeled in the CFD simulations.

The initial condition in the C2U unit has been chosen as follows: solid particles distributed evenly in the lower 70% of the C2U unit height, and the gas in the unit is 100% N₂. The void fraction of the static bed is calculated to ensure that the solid inventory matches the experimental tests (3.1 kg for AX and 1.62kg for 32D).

All simulations are performed over the adsorber part of C2U system. The grid number in the 2D axi-symmetric model is 24x360, which yields the grid size to be approximately 0.285cm in the radial direction and 0.278cm in the axial direction. This grid size is considered adequately fine when a filter model is applied for the multiphase flow problem.

The experimental parameters are provided by NETL according to the actual C2U experiment conditions, including the gas inlet parameters (flow rate, pressure, molar fractions, and temperature) and cooling oil temperature in the coils. The pressure data from C2U cold flow experiment are the quantity of interest that will be recorded and compared with the predicted pressure drop. The locations of pressure sensors along the adsorber are shown in Figure 3. The corresponding pressure sensor data measured from experiments are PDT3820 (P₁- P₂) and PDT3860 (P₂ - P₃). Note that PDT3820 data is available for all four sets of experiments, while PDT3860 data is only available for 32D cold and hot and non-reacting flow.

For a cold flow CFD case, the simulation was run for at least 200 seconds to ensure that it has reached a statistically steady state. For hot but non-reacting CFD cases, the simulations were run for 700 seconds to ensure a steady state in both hydrodynamics and thermodynamics. For the 32D reacting flow simulations, due to the continuous chemical reaction, the system will not reach complete steady state until the sorbent reaches its maximum capacity. Thus, the simulation times were set differently according to the specific time span used in each experiment. The time step can be automatically adjusted in MFIX to reflect the instantaneous hydrodynamics, reaction, and transport conditions.

4. AX Cold Flow

4.1 CFD Simulation Results for AX Cold Flow

CFD simulations were performed for the C2U unit using MFIX to systematically investigate the effects of gas flow rates on the flow hydrodynamics of the C2U adsorber system. The design of experiment was structured with the subsequent validation and calibration in mind, and the simulation initial and boundary conditions for each case are determined based on the corresponding conditions of the experimental case.

Pressure drop between two pressure differential transmitters (PDT) is one of a few quantitative physical variables that can be directly measured, and is often used as the main QOI to describe the fluidized bed. The adsorption of CO₂ onto mesoporous sorbents impregnated with amines involves a number of different complicated processes occurring at different length scales, most of which depends strongly on the local hydrodynamic characteristics of the multi-phase bubbling bed, where the pressure drop serves as one of the main quantitative measurement. For AX cold flow, the pressure drop (PDT3820) is the only measurable QOI to be validated.

All detailed geometrical and operating information were extracted from the experiment data and the data and the MFIX CFD model was constructed accordingly. The latest developer's version of MFIX of MFIX with the newly implemented Milioli filtered model was used for our validation runs. For AX runs. For AX cold flow, only the pressure drop measured by sensor PDT3820 is available for validation for validation (Pressure drop PDT3860 which is a QOI for 32D flow, was wired differently for AX flow for AX flow and is thus not validated here). As illustrated in Figure 4, the bed height of a fluidized flow is characterized by the distribution of void fraction, and this hard-to-measure quantity is closely related to the easy-to-measure quantity pressure distribution. The pressure drop along the entire reactor height is analyzed after the bed reaches a statistical steady state. To achieve a reasonable bed expansion and to obtain better agreement with the experiment, both Igci and Milioli filtered models were tested and it was found that they have similar effects on the hydrodynamics in terms of lowering the bed height and improving pressure drop predictions within the bed height. Figure 5 demonstrates these effects through the snapshots of solids density distribution and the calculated pressure drop along the reactor height. The pressure drop calculated at the location of PDT3820 is then specifically compared with its corresponding experimental measurement. Four different flow rates are considered, i.e., 15, 30, 45 and 60 slpm. All results are plotted in

Figure 6 and two major findings are summarized as below:

1. Simulation results generally agree well with the experimental data;
2. Two different filter models produce very similar predictions.

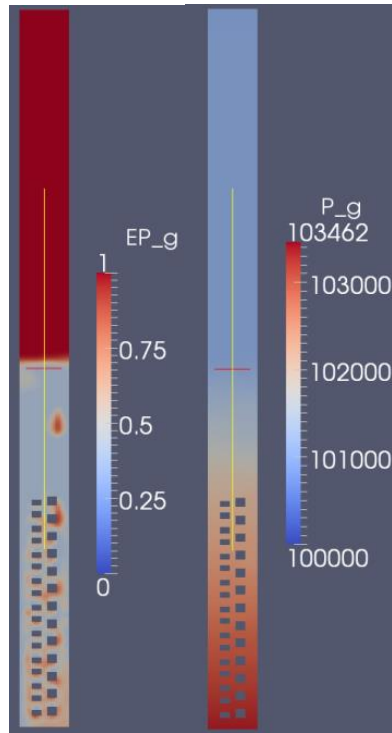


Figure 4 Snapshots of void fraction and pressure distribution for AX cold flow

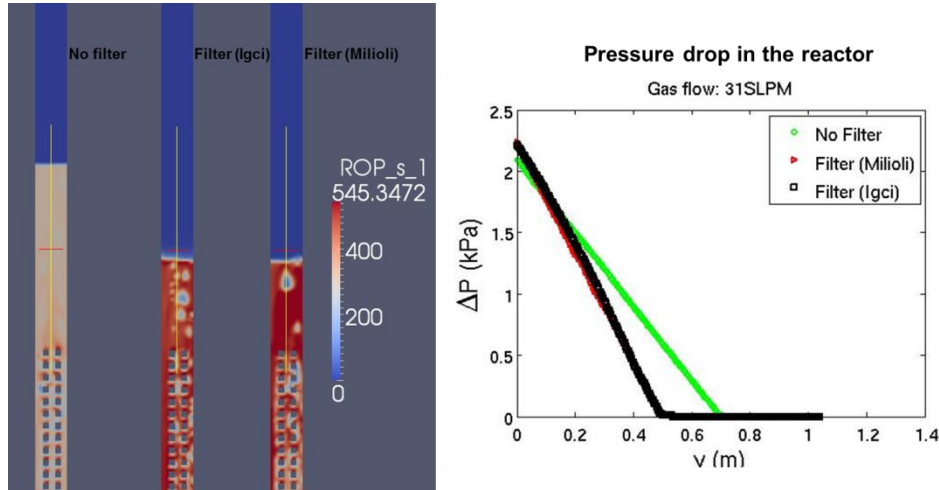


Figure 5 Snapshots of solids density distribution and the calculated pressure drop along the reactor height

4.2 UQ analysis and results for AX Cold Flow

The variables involved in the experimental data are the input variable flow rate (x), and the output variable pressure drop location PDT3820. The pressure drop output is the time averaged value of the pressure drop once it was oscillating in steady state. The PDT3820 pressure drop was measured on the physical system at 50 x -locations drawn from a LHS sample.

A total of 120 production simulation cases have been designed, run, and prepared for model validation and uncertainty quantification study. Design of computer experiments

methods have been employed to provide the most benefit to the calibration process. The MFIX model parameters involved in the calibration for this case were (θ_1) Res-PP: the particle-particle coefficient of restitution, (θ_2) Res-PW: the particle-wall coefficient of restitution, (θ_3) FricAng-PP: the particle-particle friction angle, (θ_4) FricAng-PW: the particle-wall friction angle, (θ_5) PBVF: Packed bed void fraction. These are the same parameters as those used for model calibration of the bubbling bed unit problem in Lane et.al (2013). We chose the prior distribution of the model parameters to be the same as that used in Lane et.al (2013), namely independent scaled and shifted Beta distributions were chosen for each of the five parameters dimensions such that they would agree with the expertise gained from previous analysis. We obtained a Latin Hypercube sample (LHS) of size 120 according to these distributions to fill up a five dimensional rectangular region.

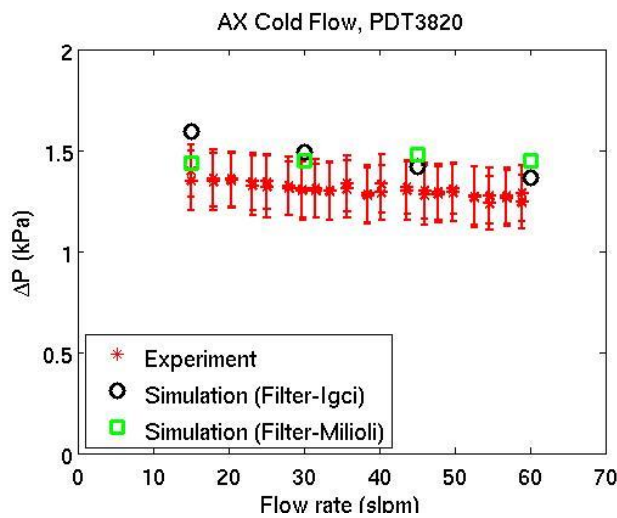


Figure 6 Validation of AX cold flow PDT3820 pressure drop

Each simulation produced (after post-processing) the output of pressure drop for a particular setting of the model parameters, and a particular flow rate (x). Therefore we had six “free parameters” for which to choose values in the LHS: $\{x, \theta_1, \dots, \theta_5\}$. The values of x were sampled uniformly in the LHS on the range [3, 40] covering the range of the experimental observations, while the other parameters were sampled according to there afore mentioned independent prior distributions.

The posterior distribution of Θ is depicted in Figure 7 by the marginal distributions of each element of Θ . Marginal distributions are sufficient to summarize the posterior distribution of Θ in this case since there was very little posterior dependency among the parameters. In Figure 7 it can be seen that the posterior distribution of the model parameters is nearly the same as the prior distribution. This indicates that there is very little information in these data to inform the “best” value at which to set the model parameters. Another way to say this is that there is very little sensitivity to the model parameters for the pressure drop at these locations. That is, setting the model parameters to any values in these ranges will produce very similar model results.

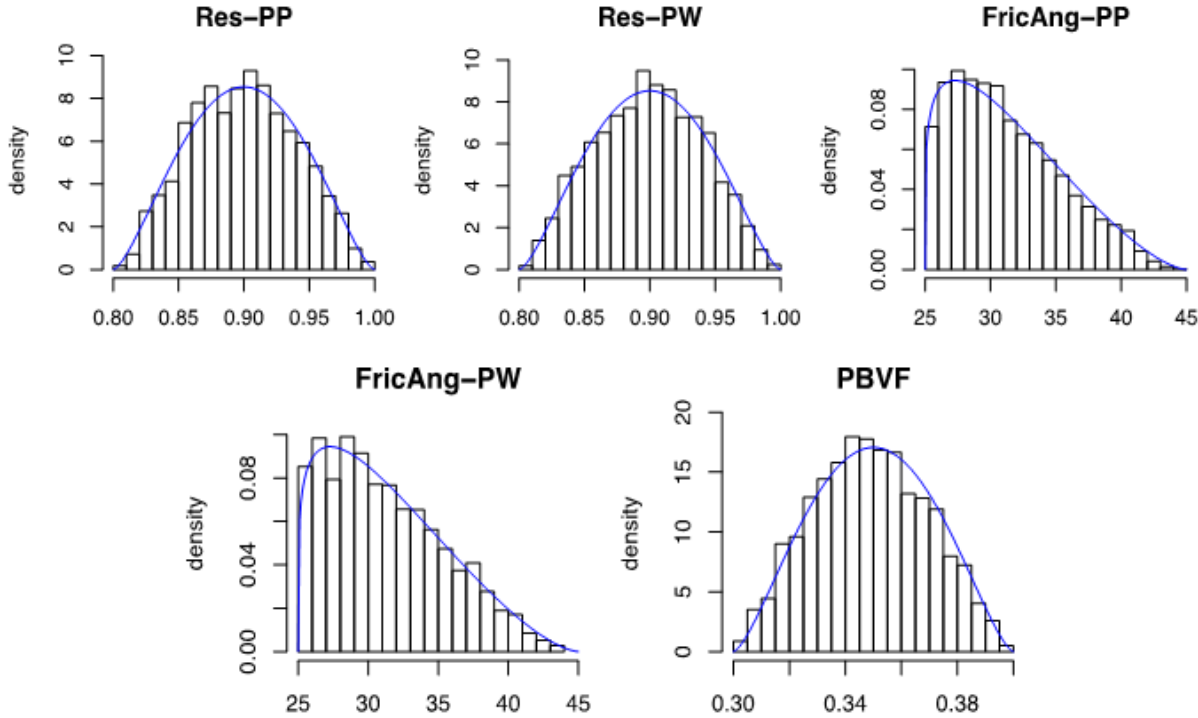


Figure 7 Marginal posterior distributions of the five model parameters (provided as histograms of the MCMC sample) along with the assumed prior distributions (blue curves)

During the work and discussion on this unit problem, it was decided that it is most appropriate to include Effective Particle Size as a calibration parameter. In principle the particle size distribution is known, but only one value (or two distinct values which results in slower run times) can be specified in MFIX. If a single size is used to describe all particles, it should probably be *close* to the Sauter Mean Diameter (SMD) of the particles, but not necessarily equal to it. Therefore, we used Sauter Mean Diameter (SMD=115 μm) and pilot runs to develop a prior distribution, and another LHS design of MFIX runs was made, including varying particle sizes. The resulting posterior distribution is provided in Figure 8. The model results are very sensitive to particle size. The most likely particle size according to the calibration is $\sim 117 \mu\text{m}$.

Figure 8 also provides posterior fitted curves for the pressure drop PDT3820 output. This plot provides predictions across flow rate. The posterior mean curve is provided as a thick blue line. Five hundred posterior prediction realizations of the simulator only are provided by the light blue curves. These realizations include the uncertainty in both θ and the emulator approximation of the simulator. These posterior realizations are barely noticeable in the plot indicating very little variation off of the mean curve. The edge of these posterior realization curves can be considered a 1/500 confidence boundary of possible simulator results.

The thick red curves in Figure 9 are posterior mean curves of the emulator predictions plus the model discrepancy (i.e., prediction realizations of the actual physical system), while the light red curves are again 500 posterior realizations emulator predictions plus the model

discrepancy. The result also provides measurement error bounds. Note that these error bounds are for the *mean* pressure drop once in steady state, not for the individual observations in time as pressures oscillate in steady state. The quantity predicted by both the red and blue curves is the mean pressure drop so the error bounds for the mean pressure drops are relevant here. Notice these measurement error bounds are not all that visible, since they are very tight, but they are nonetheless being plotted. It is also clear that by including size the model captures the trend of pressure drop versus increasing flow rate much better, and there is also more uncertainty in the simulator predictions since the model is sensitive to size.

In summary, there was very little sensitivity of the model output (mean pressure drop in steady state) to these model parameters. This may or may not be the case for other C2U experimental setups or other system modeling scenarios. There is some discrepancy from model to data for the mean pressure drop in steady state at PDT3820, but it is relatively small.

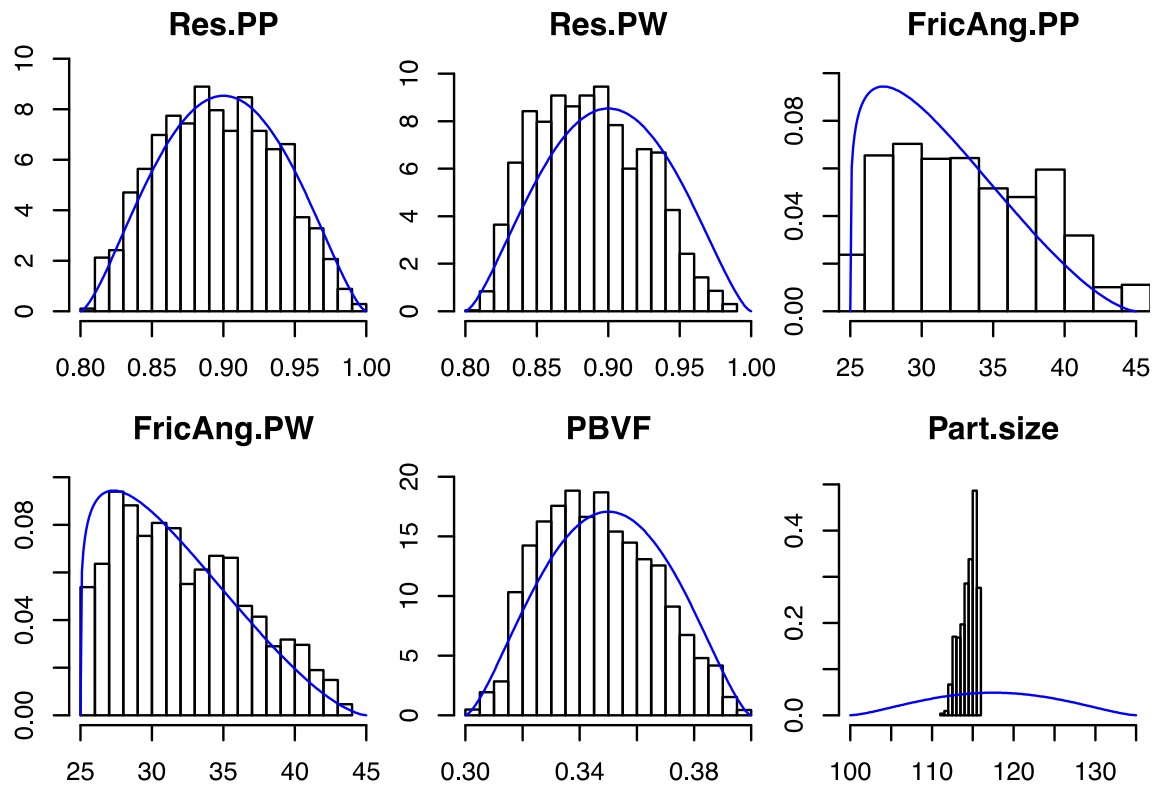


Figure 8 Marginal posterior distributions of the six model parameters (now including effective particle size) for the AX cold flow unit problem.

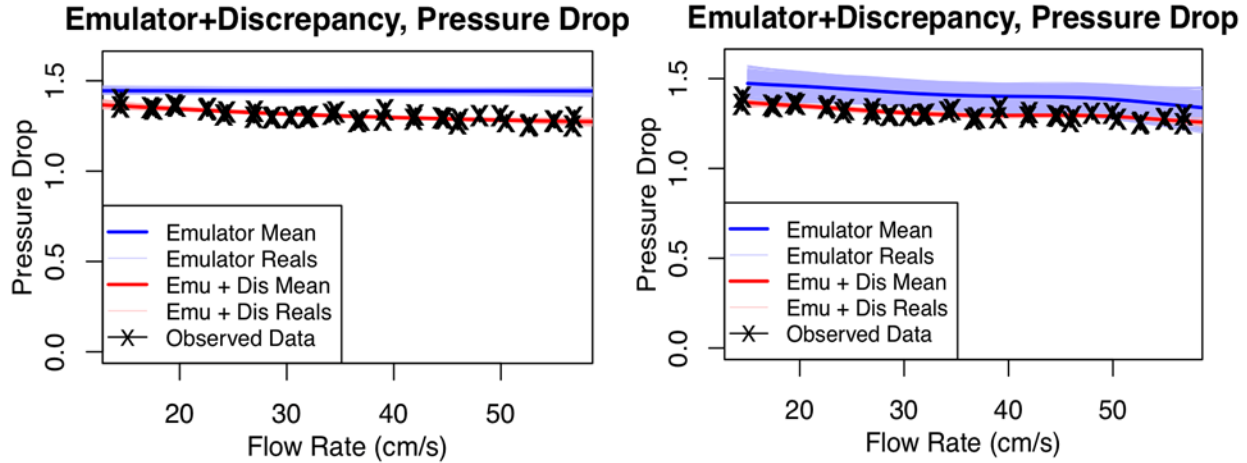
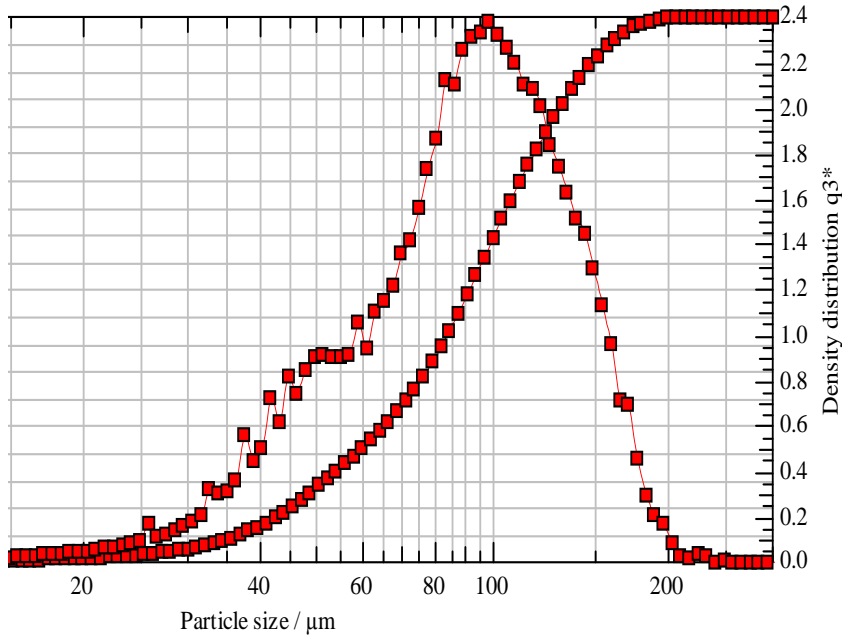


Figure 9 Experimental pressure drop data at PDT3820 across flow rate, along with posterior emulator results and emulator plus discrepancy results for model without particle size calibrated (left pane) and model with particle size included in the calibration (right pane). The light colored lines are posterior realizations, while the thick line is the posterior mean curve. Black vertical lines are error bars for the steady state mean pressure drop for each experimental data point.

5. 32D Cold Flow

5.1 CFD Simulation Results for 32D Cold Flow

The model setup, as described above for AX cold flow, was modified by replacing the particle properties with those of 32D, including particle size, density and total mass. Due to the maturity issues with the newly implemented Milioli filter model, the more stable Igci filter model is used in the MFIX simulations. The pressure drop measured at sensor location of PDT3820 in the experiment is taken to be the quantity of interest for this validation. From the validation of AX cold flow, we found that the Sauter Mean Diameter (SMD) of the sorbent population cannot be used as the effective particle size in MFIX in order to accurately capture the measured pressure drop over the flow rates considered. In fact, the measured 32D particle size distribution was bimodal (see Figure 10) and its overall SMD might be misleading. Moreover, elutriation was observed during the experiments, and fresh particles were replenished. Hence effective particle size was also added as an additional calibration parameter for 32D validation.

**Figure 10** Sorbent 32D particle size distribution

5.2 UQ Analysis and Results for 32D Cold Flow

The general Bayesian calibration/ model assessment methodology, BSS-ANOVA-UQ, was once again used to calibrate/validate the MFIX CFD model on this unit problem. The effective particle size was also included as a model calibration parameter in this case.

In this case $SMD = 75 \mu\text{m}$, however, as mentioned above the 32D size distribution was bimodal and overall SMD is misleading. In this case the most appropriate single value to use should be *close* to the Sauter Mean Diameter (SMD) of the *larger* cluster of particles, but not necessarily equal to it. Thus, we fit a two-mixture normal distribution to the particle size distribution to obtain the distribution of the *large* particles. We then used the $SMD = 102 \mu\text{m}$ of this large particle distribution along with several scouting runs to inform a prior distribution for effective size. The resulting posterior distribution is provided in Figure 11. The most likely value according to the calibration is $\sim 115 \mu\text{m}$, but with more uncertainty than for AX. The additional uncertainty compared to AX is possibly due to the different filtered model used here (Igci instead of Milioli), and/or the more complicated bimodal nature of particle size distribution for 32D. Figure 12 displays the fitted emulator and emulator plus discrepancy curves to the PDT3820 pressure drop against gas flow rate. There is generally very good agreement (within experimental error) from the emulator to the data, leading to a small/negligible model discrepancy in this case.

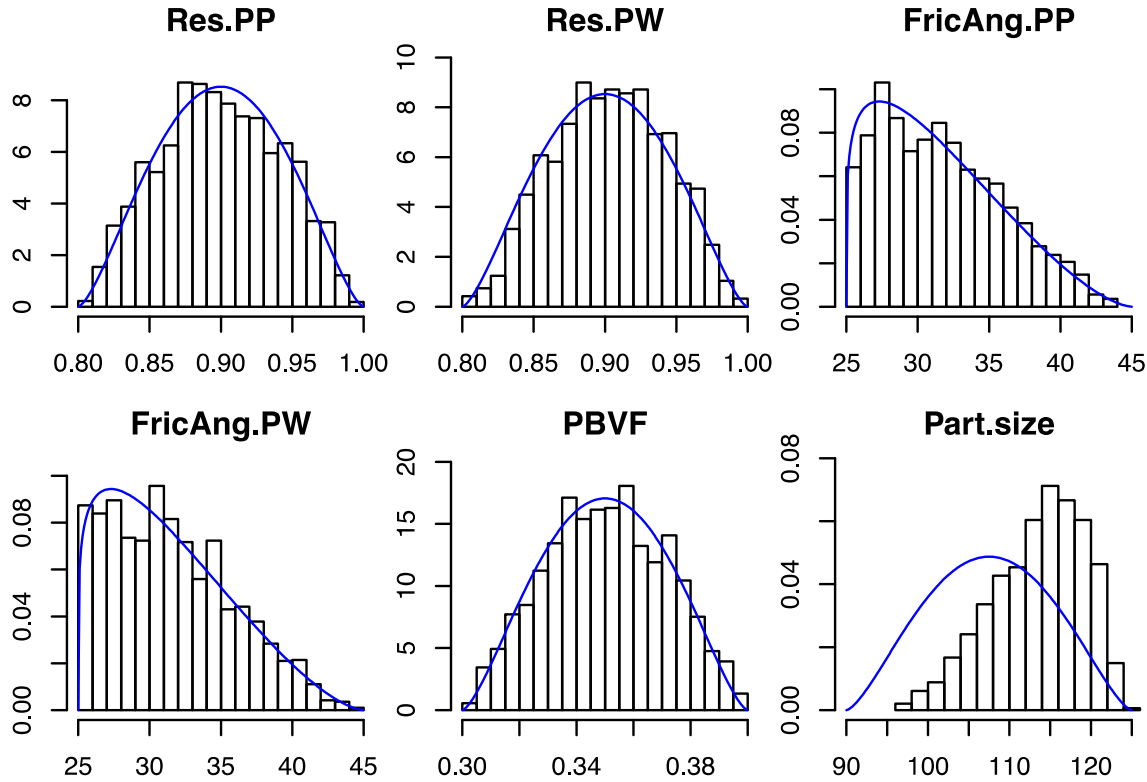


Figure 11 Marginal posterior distributions of the five model parameters resulting from the 32D cold flow unit problem (provided as histograms of the MCMC sample) along with the assumed prior distributions (blue curves)

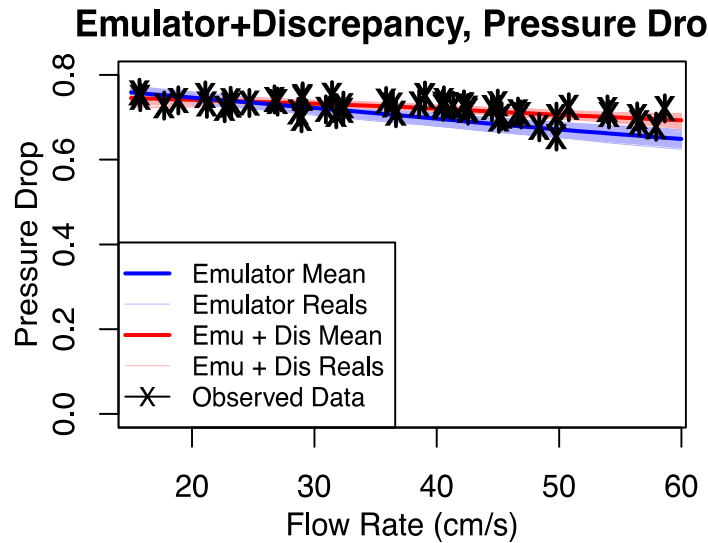


Figure 12 Experimental pressure drop data at location PDT3820 across gas flow rate, along with posterior emulator results and emulator plus discrepancy results. The light colored lines are posterior realizations, while the thick lines are posterior mean curves. Black vertical lines are error bars for the steady state mean pressure drop for each experimental data point.

6. 32D Hot Non-Reacting Flow

6.1 CFD Simulation Results for 32D Hot Non-Reacting Flow

In this unit problem, the heat exchange coils act as not only the no-slip boundaries for hydrodynamics but also as the heating boundaries for thermal kinetics. All the temperature setting information, including coil temperature and inflow gas temperature were extracted from the experiment data and were then input into the MFIX model accordingly. Same as for 32D cold flow cases, the Igci filter model is used in the simulations. In the experiment, the bed temperatures were measured at thermal couples of TE3962A and TE3965, and their values were averaged as the QOI for thermal kinetics validation. The pressure drops measured at both PDT3820 and PDT3860 were available for hydrodynamics validation. As the nominal validation study preceding the formal calibration process, eight cases from the experimental data were selected to cover the whole range of flow rates (15- 60slpm) and temperatures (40-80°C). The steady state of hydrodynamics is reached after 100s; however, the thermal kinetics reaches its steady state after 700s. The validation of steady-state temperatures in different cases is summarized in Figure 13 (a), while pressure drops are shown in Figure 13 (b). Two different particle sizes are considered to address the effect of particle size on hydrodynamics. Three findings are summarized as below:

1. Simulation results have good agreement with the experimental data;
2. Particle size has a significant effect on pressure drop, and a calibration procedure including particle size is essential in our high fidelity CFD validation;
3. The thermal boundary condition imposed on coils accurately captures the thermal kinetics.

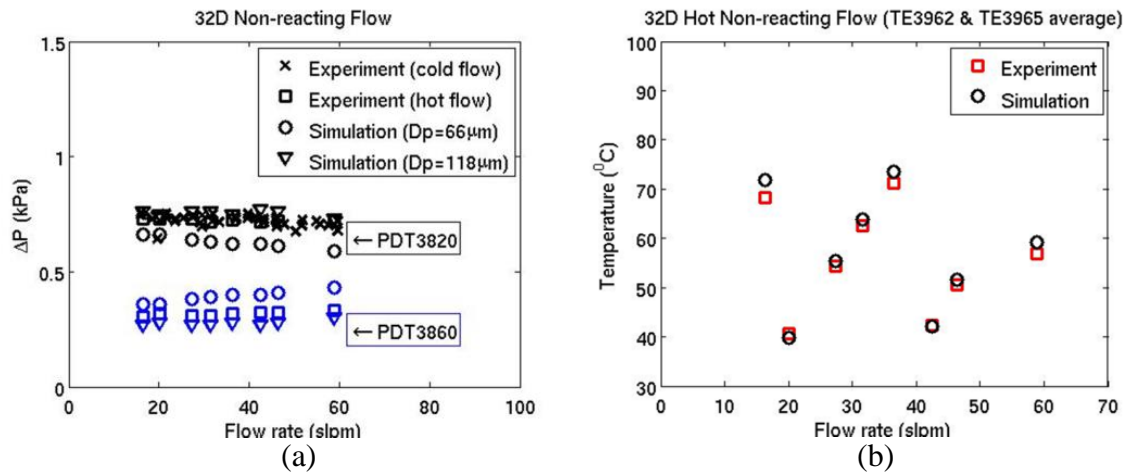


Figure 13 32D Hot Non-Reacting Flow Validations

To further examine the thermal transients in addition to the steady-state temperatures, temperature histories were also calculated and compared with the experimental measurements. A customized code of applying variable boundary conditions was developed to facilitate this purpose. Specifically, the varying boundary conditions include the inlet gas flow rate and the temperature of oil circulating in the cooling coils, as shown in Figure 14.

Figure 15 shows the predicted temporal bed temperature from the simulations, which matches well with that of experiments in terms of both values and trend.

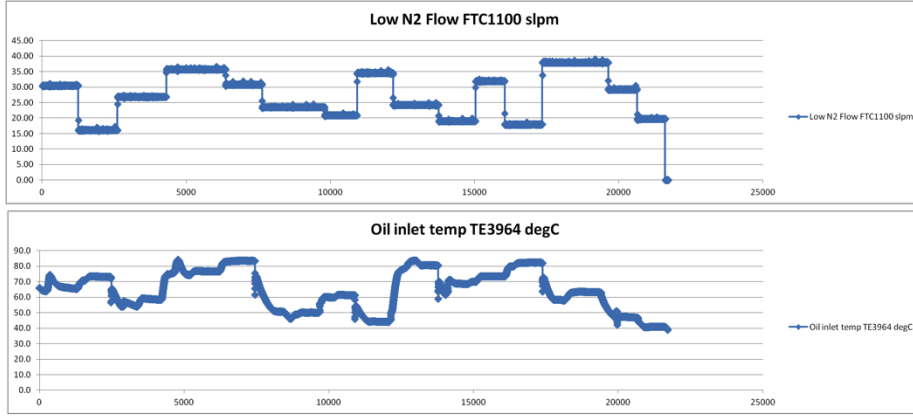


Figure 14 Time-varying boundary conditions

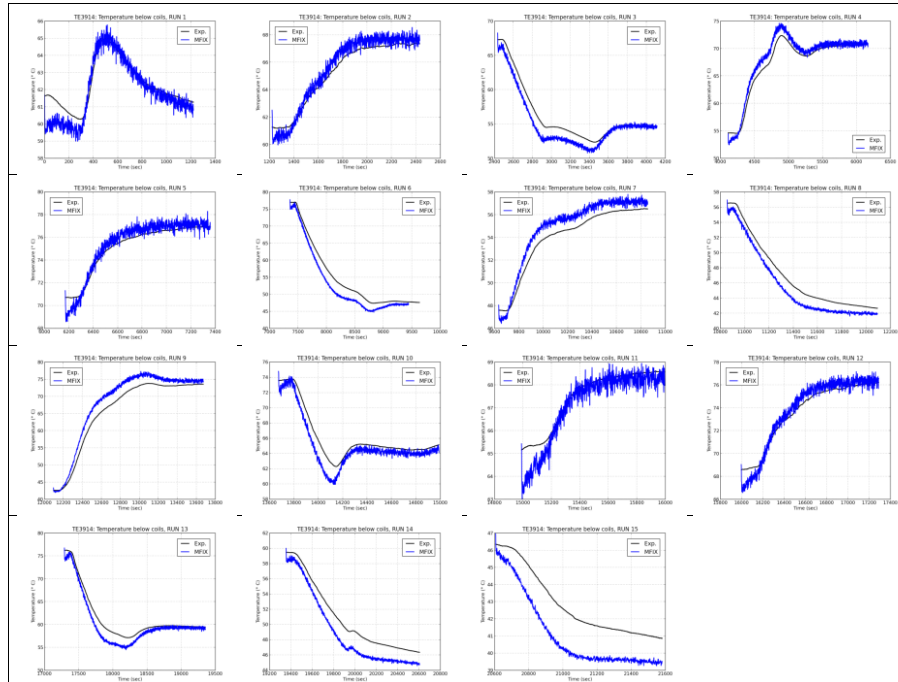


Figure 15 Bed temperature vs. time

6.2 UQ Analysis and Results for 32D Hot Non-Reacting Flow

The same BSS-ANOVA calibration procedure with LHS sampling for simulation runs was used for this unit problem as well, however, there are now two inputs (flow rate and bed temperature). Pressure drop PDT3860 was also used in the calibration in addition to PDT3820. Particle size was included as a parameter in the calibration with prior distribution provided by the *posterior* distribution from the 32D cold flow calibration results. The resulting posterior distribution of model parameters is provided in Figure 16. Once again, none of the model parameters (except particle size) exhibited significant changes from the

prior in their prior distribution, indicating a lack of sensitivity of pressure drop to any of these model parameters.

The fitted plots of the emulator evaluated at parameter values from the posterior distribution are provided for each output in Figure 17 and Figure 18. These plots show the respective pressure drop as a function of flow rate (for several levels of the second input, bed temperature). While there is some model discrepancy, it is once again relatively small in absolute magnitude and the model is representing the experimental reality well.

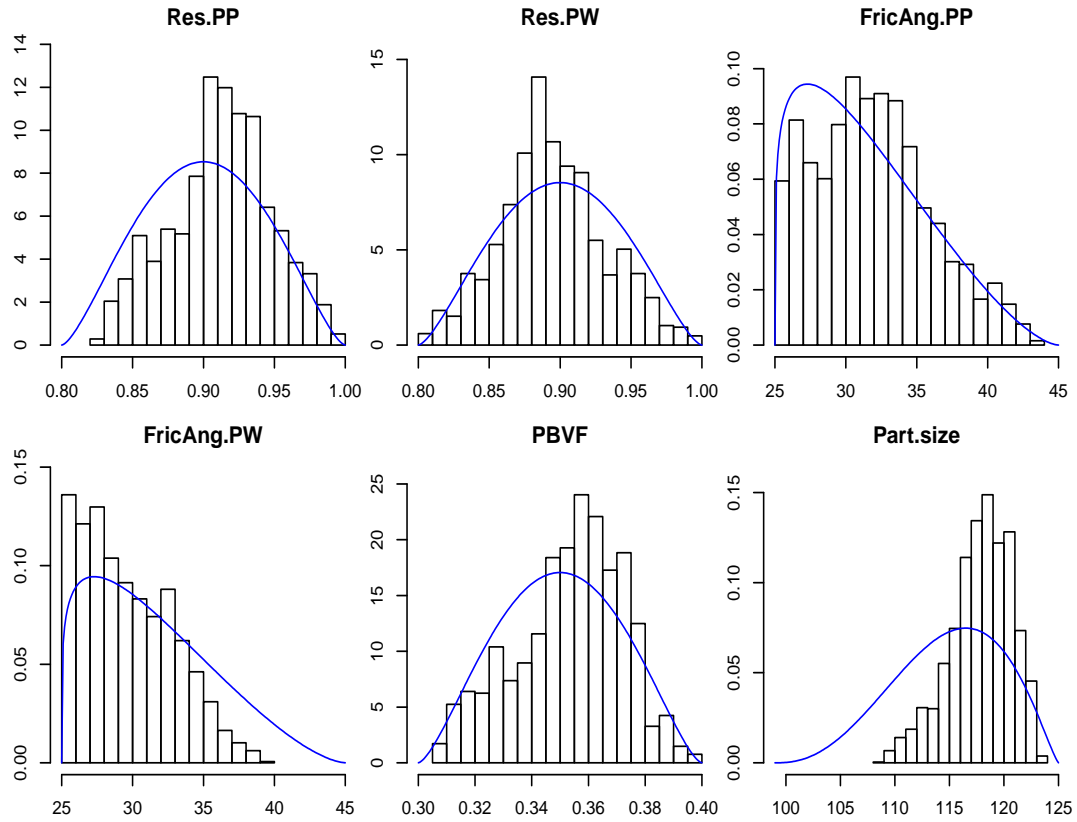


Figure 16 Marginal posterior distributions of the six model parameters for MFIX, including particle size, resulting from the 32D hot/non-reacting flow calibration.

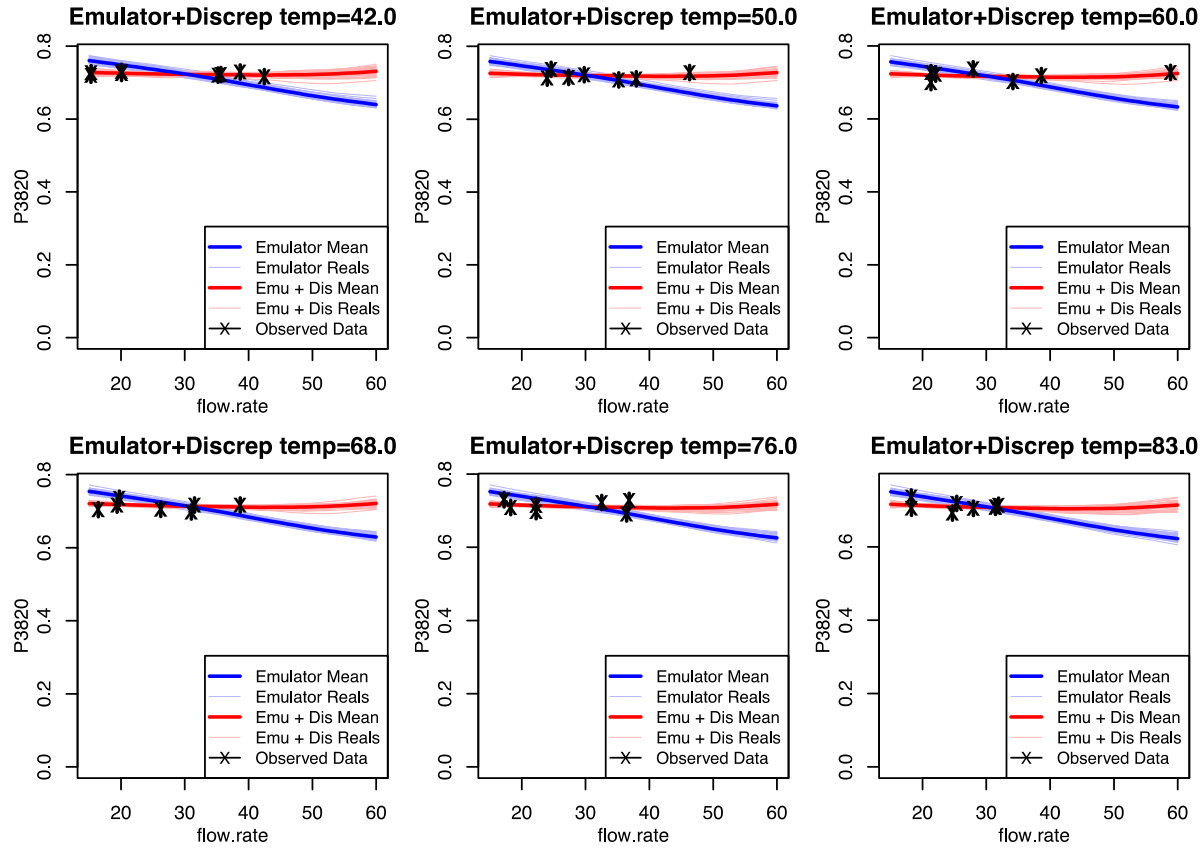


Figure 17 Fitted plots for pressure drop at location PDT3820 . Blue is model prediction, red is model plus a model discrepancy correction. The model predicts the data relatively well as the model discrepancy is not prominent here.

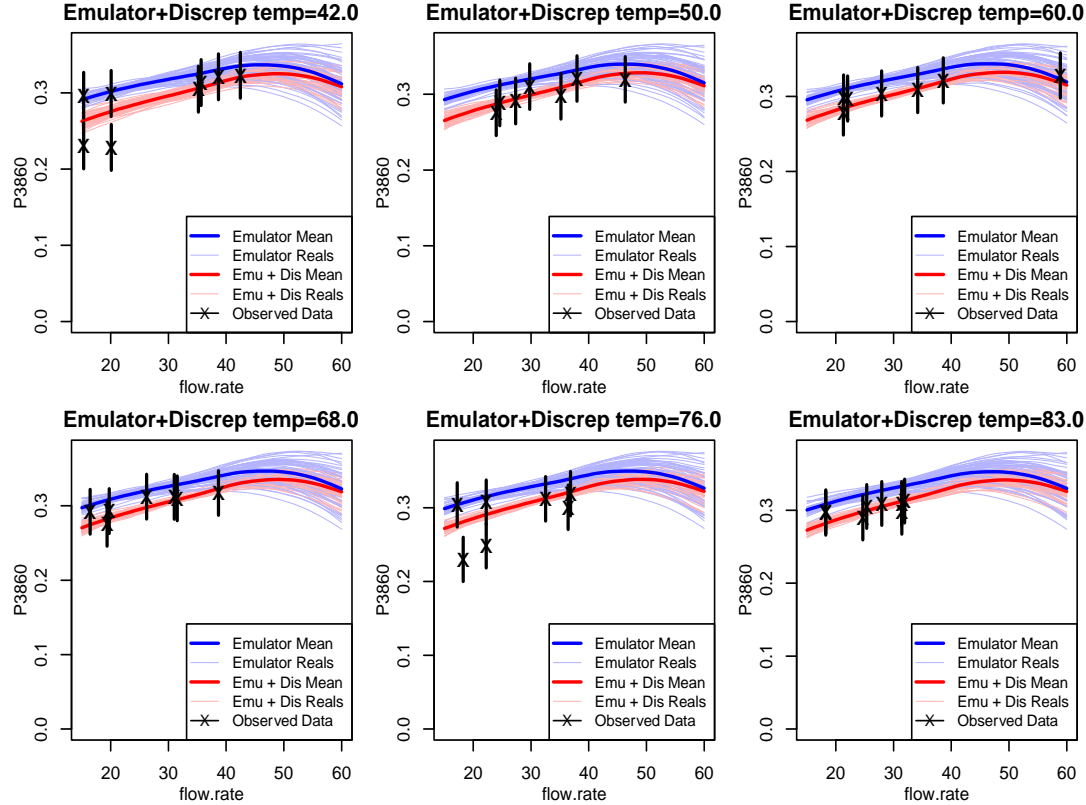


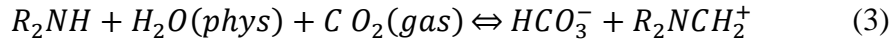
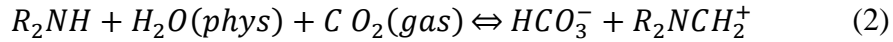
Figure 18 Fitted plots for pressure drop at location PDT3860 . Blue is model prediction, red is model plus a model discrepancy correction. The model predicts the data relatively well as the model discrepancy is not prominent here.

7. 32D Reacting Flow

7.1 CFD Simulation Results for 32D Reacting Flow

According to the validation hierarchical design, once the cold flow and hot non-reacting flow cases are validated, chemical reactions are introduced to the multi-phase flow as the coupled bench scale validation problem.

Three main reactions occur in the process of 32D adsorbing carbon dioxide.



Eq. 1 is for dry adsorption, denoted as x , Eq. 2 is for wet reaction, denoted as b , and Eq. 3 water physisorption denoted as a . The chemical reaction rates for all three are listed as follows:

$$\frac{\partial x}{\partial t} = k_c(s^2 p_c^m - \frac{xw}{K_c}) \quad (4)$$

$$\frac{\partial b}{\partial t} = k_b \left(sap_c - \frac{bw}{K_b} \right) \quad (5)$$

$$\frac{\partial a}{\partial t} = k_h(p_h - \frac{a}{K_h}) \quad (6)$$

Where

$$K_q = e^{\frac{\Delta S_q}{R}} e^{\frac{-\Delta H_q}{RT}} / P \quad (7)$$

$$k_q = \zeta_q e^{\frac{-\Delta H_q^*}{RT}} / P \quad (8)$$

The detailed formulations and parameter definitions are included in Mebane et al. (2012). The chemical reaction and equilibrium constants are determined by the following 4 parameters: ΔH , ΔS , ΔH^* , and ζ . Table 1 lists those parameters that determine the basic kinetics of the above three chemical reactions. The data was provided by task 2 basic data analysis team based on their most recent TGA data analysis. It should be noted that contributions of intra-particle diffusion were not considered in the development of these kinetic parameters since statistical methods were to be used to account for any discrepancies from the experimental data.

Table 1 Parameters for 32D Kinetics

	ΔH	ΔS	ΔH^*	$\log_{10}\zeta$
Dry Adsorption	-71649	-200	78728	3.3115
Wet Adsorption	-98828	-246.76	67960	4.2881
Water Physisorption	-87733	-260.83	11360	0.6165

MFIX tool built with custom implementation of the above 32D kinetics has been used for the multi-physics CFD simulations. Same as in previous 32D simulations, the Igci filter model is chosen.

Pressure, bed temperature, and CO₂ adsorption are the three QOIs for 32D reacting flow experiments and validation studies. The pressure distribution and its spatial and temporal variations are the best QOI to describe a fluidized bed. The bed temperature and its temporal variation best describe the heat transfer and the efficiency of cooling coils in controlling bed temperature. CO₂ adsorption is measured by the CO₂ content in the exit of the C2U unit. The CO₂ concentration in the inlet synthetic flue gas is set as designed, and the difference

between the exit CO₂ concentration and the fixed inlet value is considered adsorbed by the sorbent.

We have also performed extensive studies on the particle size of 32D sorbent, which is specified as 118 μm by the manufacturer in as-received condition. The sorbent particles had been in storage for several months prior to the experiments. During experiments, particle elutriation was observed. The elutriated particles were replenished by fresh particles with the equivalent weight before each run. At the end of each experimental day, sorbent samples were taken from the C2U unit for particle size analyses. The SMD (Sauter mean diameter) for the used sorbent is found to be in the range of 80-90 μm with a bi-modal distribution. See Figure 10. Since implementation of the actual particle size distribution in MFIX is not straightforward, previous calibration studies (see Sections 5.2 and 6.2) were leveraged here where we found that 118 μm is a more plausible particle size as the simulations generate a more consistent fluidized bed results compared with experiment measurement.

Among the three QOIs being validated, pressure drop and bed temperature predicted in the simulations are both consistent with the experiment data, as we have presented in the previous three validations. For 32D reacting flow, the new important QOI is the CO₂ adsorption, which can be quantified in two terms: the overall CO₂ adsorption capacity and the adsorption kinetics of the reactor in the temporal space, i.e., the breakthrough curve, see Figure 19.

Experimental Run#2 was chosen as the nominal experiment run for our initial validation effort. The experimental breakthrough curve shows some initial period of steady CO₂ adsorption followed by a relatively fast decay, while the simulation with original kinetics parameters derived from TGA fit shows a higher initial CO₂ leak rate, a relatively slower CO₂ breakthrough rate, and a longer tail leading to final adsorption capacity. The total CO₂ adsorption capacity, which is equivalent to the area underneath the curves, is consistent with experiment value.

Note that the influences of fine, unresolved flow structures in our simulations are captured via filtered sub-grid constitutive relations (Igci et al., 2008; Igci and Sundaresan, 2011). However, using the filtered models, the predicted strain rates are larger than expected, especially for the solids phase, leading to extremes in solid and gas velocities. This behavior strongly suggests that the filtered magnitude of solids viscosity is insufficient to match the dissipation occurring in reality, and a further increase of the effective solids viscosity is required. Through in-depth numerical analysis and calibrations, it is found that increasing the solid viscosity by 10 times and simultaneously increasing the reaction rate by 100 times brings the CO₂ breakthrough curve closer to experimental observation (Figure 19). This is consistent with a process which is diffusion controlled as described by Monazam et al. (2013). Increasing solids viscosity makes particles move more homogenously, i.e., it prevents the unphysical extremes in velocities for both solid and gas phases. This results in better flow characteristics, as would be expected in experiments, and thus a better adsorption profile.

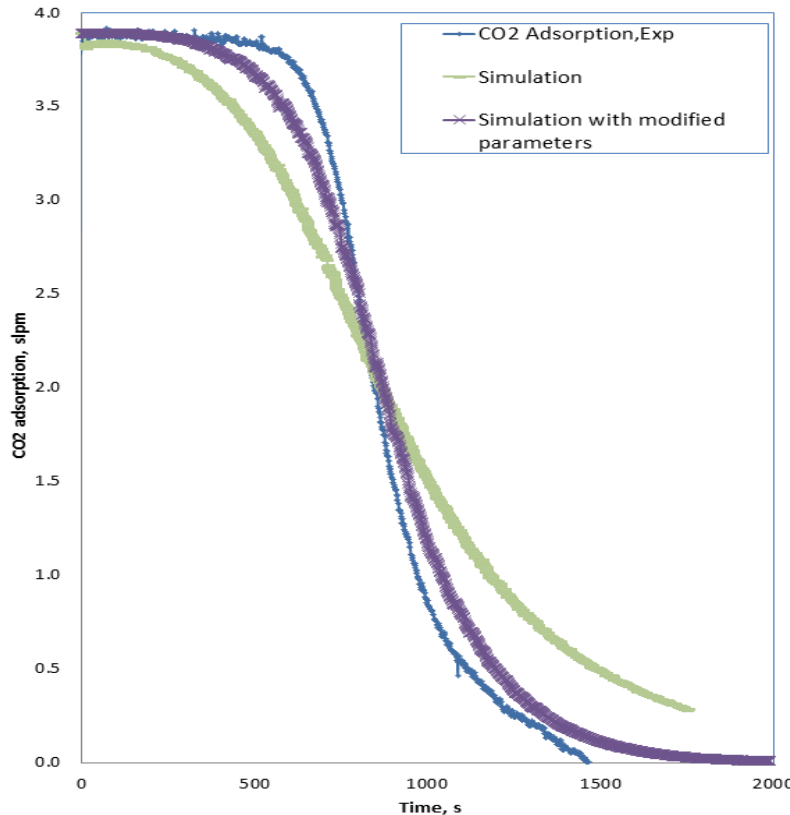


Figure 19 CO₂ adsorption curve for run #2

However, increasing solid viscosity requires a further lowering of the simulations' residual tolerances to prevent solids mass loss due to numerical errors, which greatly increases the computational cost. Through numerous simulation tests, it is found that setting the effective viscosity to 2 times the original (filtered) value and effective reaction rate to 100 times the original value is the best compromise: an acceptable breakthrough curve is obtained within a reasonable computing time. Although our adjustment of the solids viscosity is an engineering approximation, these findings show that further refinement of the filtered stress models is warranted.

It was observed by the experiment task that the capture capacity reduces gradually after each of the adsorption-regenerating cycle, as shown in Figure 21. The curve fit indicates an estimated 0.27% decay in each run. In the MFIX models, amine molar fraction is reduced by the same percentage in each run in the chronological order to reflect this possible sorbent chemical degradation.

Seventy one MFIX simulations have been performed with corresponding experimental operating conditions in this validation exercise. Figure 20 depicts the distribution of 4 operating parameters: gas flow rate, gas inlet temperature, gas CO₂ concentration, and the cooling coil temperature. The experiments were carefully designed to maximize the coverage in all possible realistic CO₂ adsorption operating space.

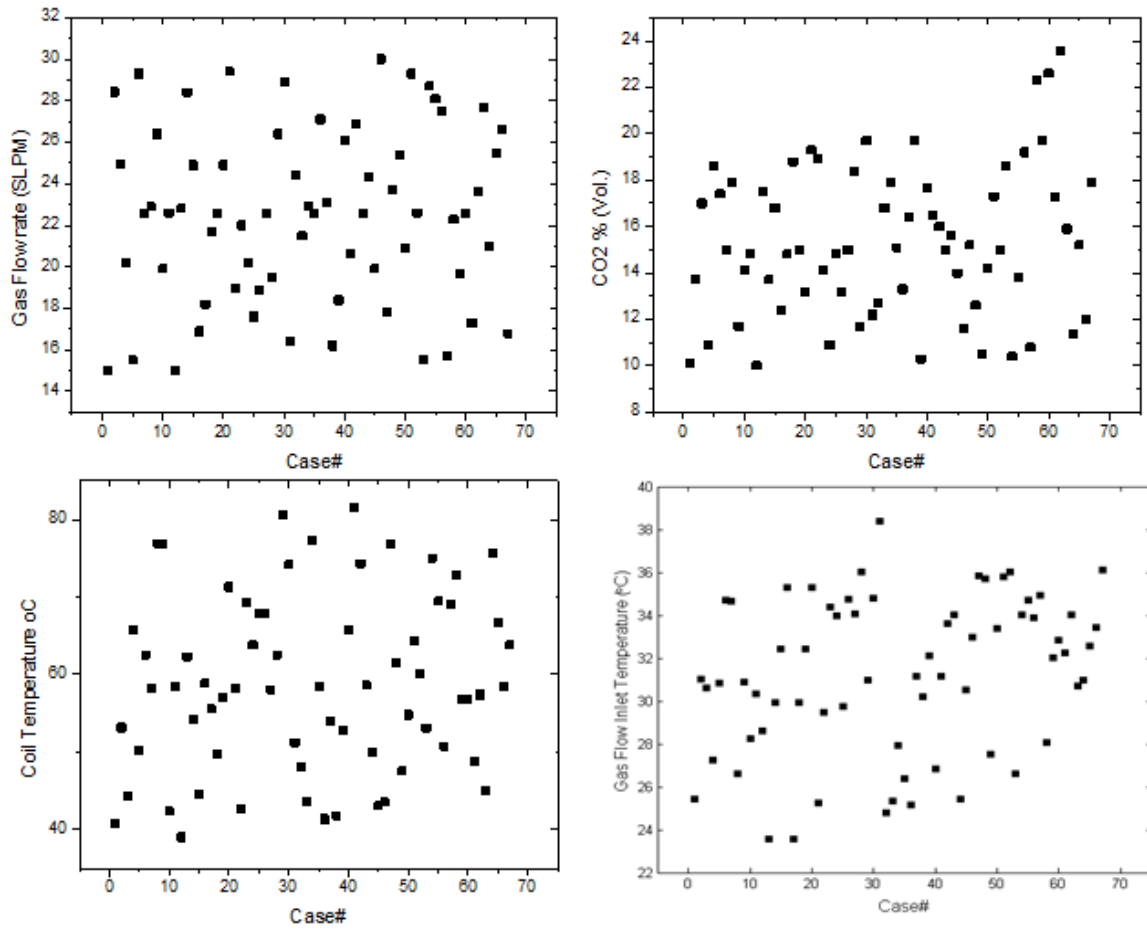


Figure 20 Distribution of experiment parameters

Simulations for all 71 experiment runs have been performed, with the boundary and initial conditions matching exactly to the experiment conditions.

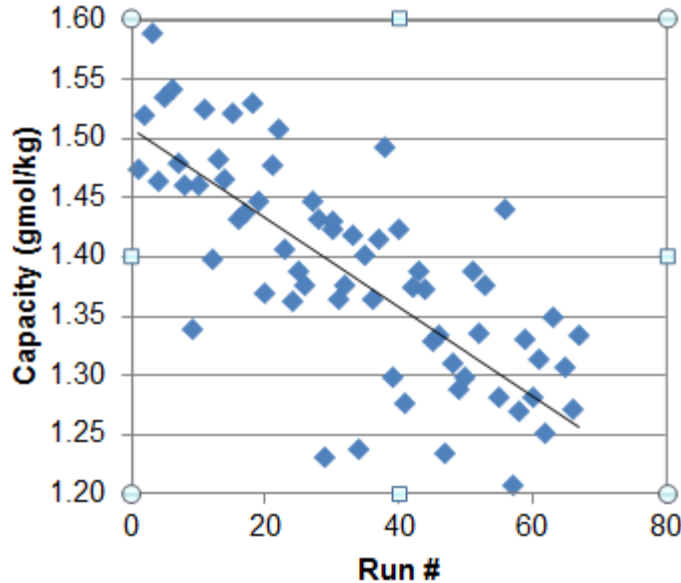


Figure 21 Experiment data shows decrease in CO₂ adsorption capacity over time

A direct comparison between the experimentally measured bed pressure drop and the simulated pressure drop for all 67 cases is presented in Figure 22(a). Reasonable comparisons have been achieved, with predicted pressure ranges larger than the measured ones. In order to gain more insights into the simulation and experiment data, we plot the simulation results versus the experiment data as shown in Figure 22(b). Ideally, the perfect simulation and experiment results should fall on the straight line with a slope of 1, the black line in Figure 22. In this case, the predicted bed pressures scattered around the black line at lower pressure levels, the predicted pressures are higher than the actual measurements at higher pressure levels.

The bed temperature predicted by the simulation matches remarkably well with the experiment measurement, as shown in Figure 23 in a similar manner. This demonstrates that the modeling of cooling coils as separately boundary condition regions has accurately capture the heat transfer within the reactor. Average temperature for both coils and the bed are taken in the comparison. The time-dependent values are available, and a custom made MFIX can simulate time-dependent variable boundary conditions (Section 6.1). For computational efficiency, however, this more complicated approach was scouted but not chosen for the production runs. Figure 23 (b) shows all data from experiment and simulated bed temperature falling in a rather narrow range around the line with a slope of 1.

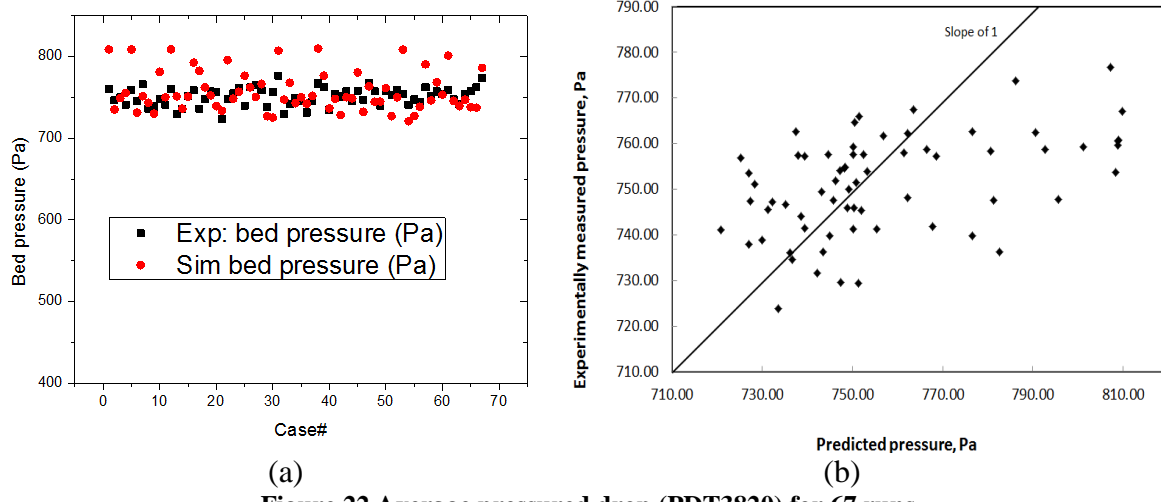


Figure 22 Average pressured drop (PDT3820) for 67 runs

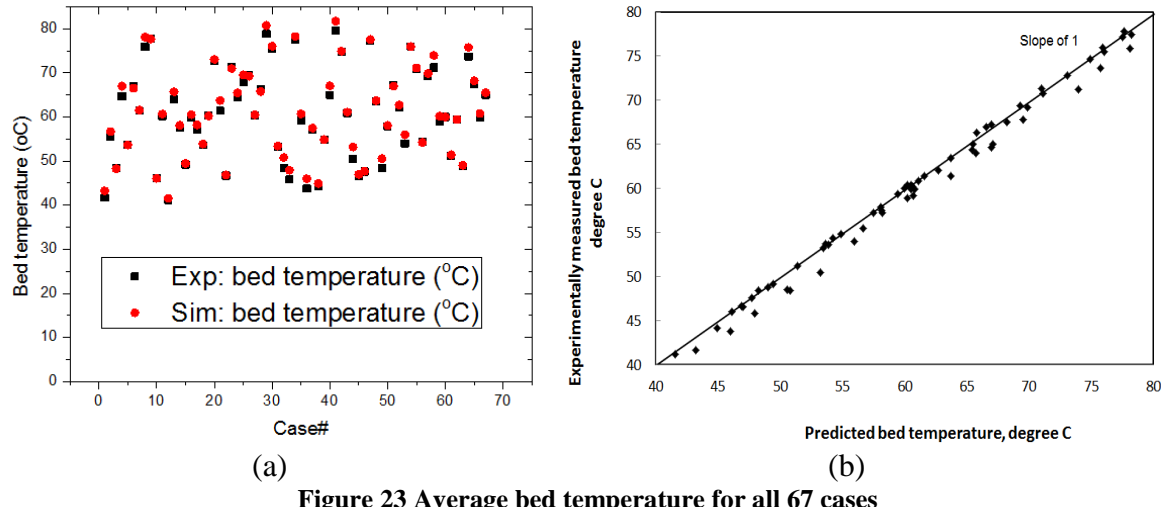


Figure 23 Average bed temperature for all 67 cases

Figure 24 (a) and (b) describe the comparison of CO₂ adsorption between experiment and simulation results. Results in Figure 24 (b) indicate that at low capacity, the model under predicts the overall CO₂ adsorption; while at high capacity, it over predicts.

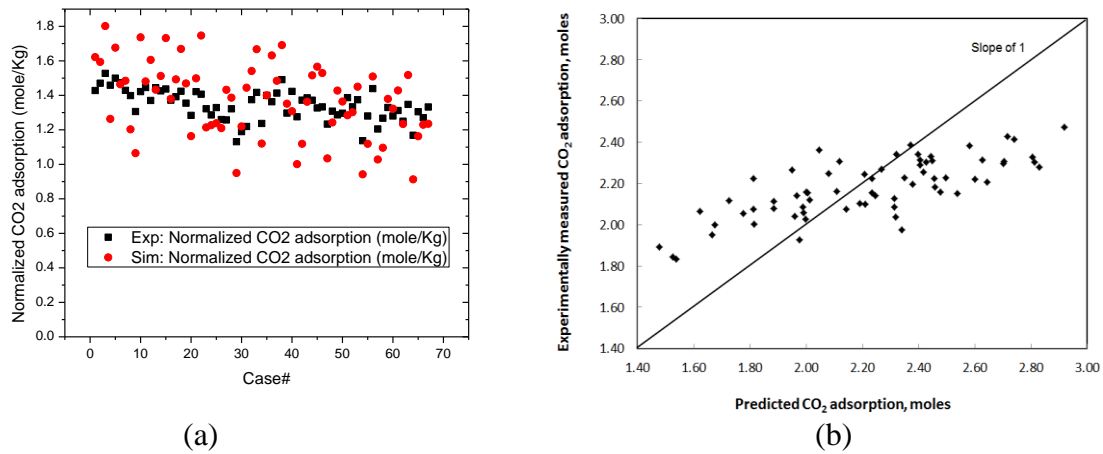


Figure 24 Normalized CO₂ adsorption for all 67 cases, and comparison with experiment data

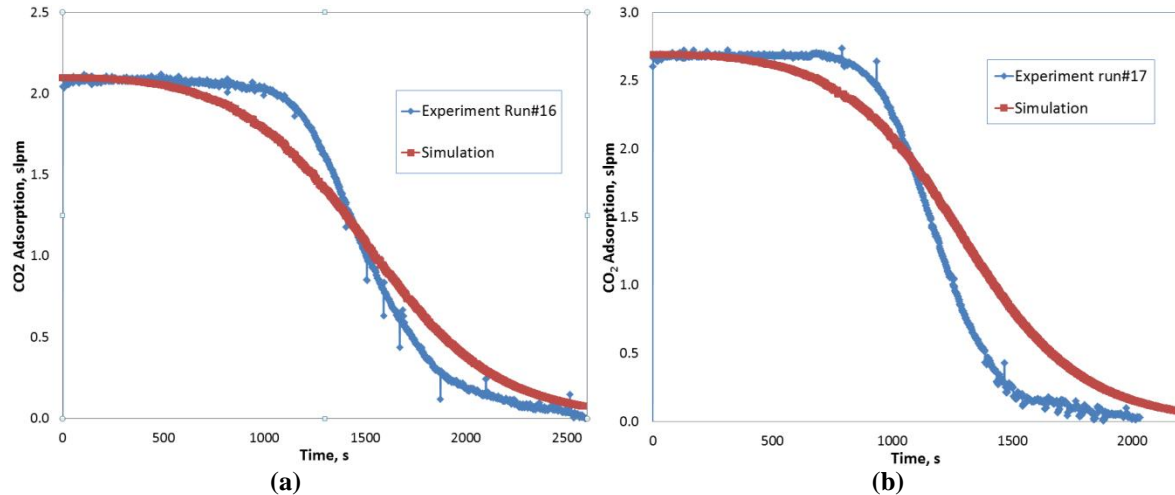


Figure 25 CO₂ adsorption breakthrough curve

Figure 25 (a) and (b) show the CO₂ adsorption breakthrough curves for two experiment runs, #16 and #17 respectively. It can be observed from the comparisons that the predicted overall CO₂ capacity (equivalent to the total area under the curve) is very close to that of the experiment data. On the other hand, while the experimental data show a more sudden drop of CO₂ adsorption rate after an initial steady region, the simulation results start the adsorption decay much earlier with more gradual decay.

To quantitatively describe the CO₂ adsorption kinetics, the time needed to adsorb a certain fraction of the total adsorption capacity is defined. Note that the total capacity measured in the experiment is used as the common reference. For example T_{25%} is the time for the C2U system to adsorb 25% of the total capacity. Figure 26 shows the comparison on T_{25%} and T_{50%}. The time difference is negligible, reflecting the fact that early adsorption breakthrough curves from the simulation matches well with that of the experiments.

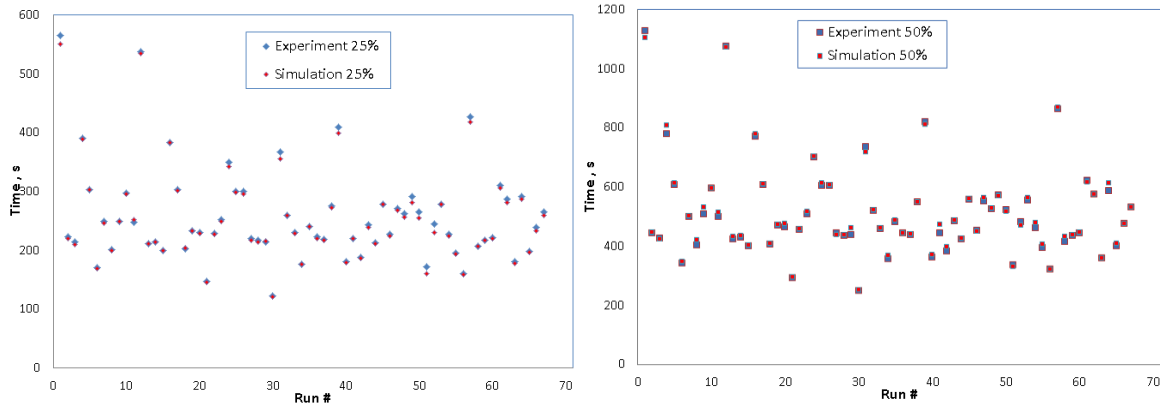


Figure 26 Time for C2U unit to adsorb 25% and 50% of total capacity

Figure 27 shows $T_{75\%}$ comparison. In general the simulation time is larger than the experiment counterpart, reflecting the earlier adsorption rate drop in the simulations. Consistency has been achieved for most runs.

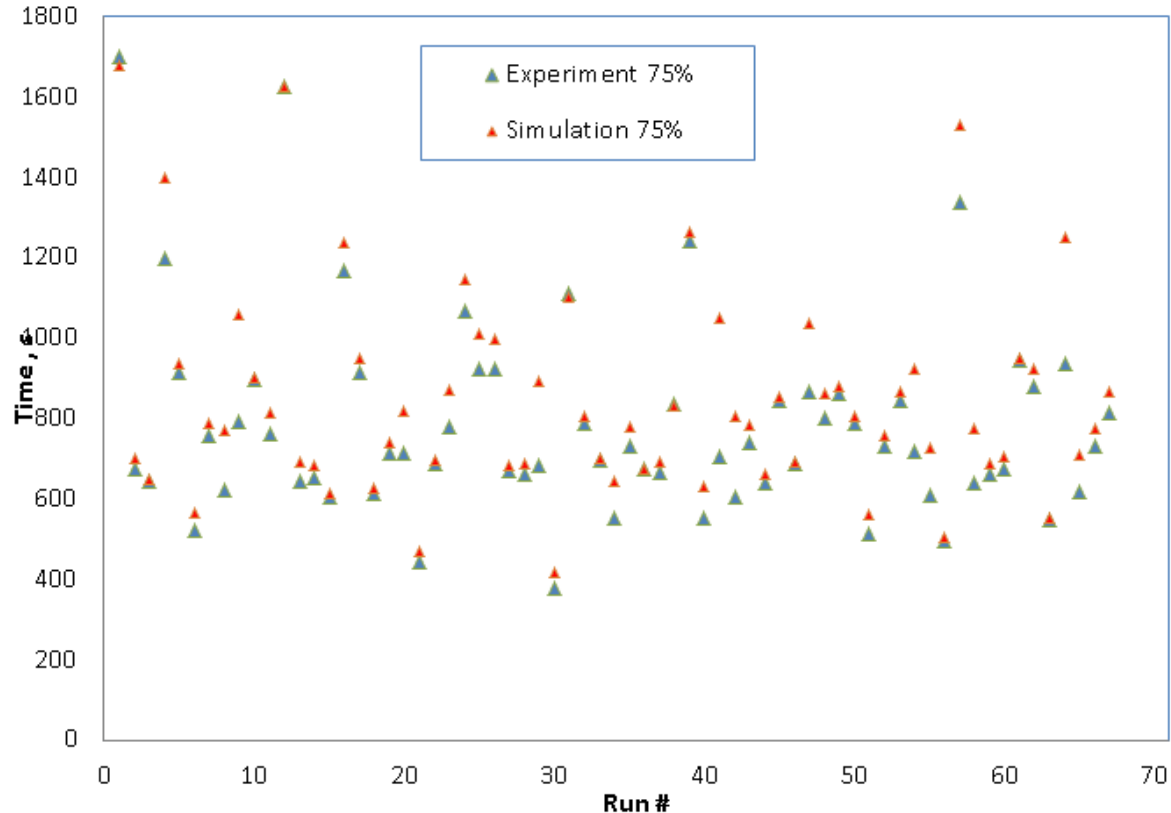


Figure 27 Time for C2U unit to adsorb 75% total capacity

Figure 28 presents the comparison between simulated adsorption time and experiment adsorption time for 25%, 50%, and 75% adsorption, respectively. Again, it was confirmed that the simulation results are in very good agreement with the experiment result for adsorption percentage of 25% and 50%, respectively. There is increasing discrepancy between simulation and experiment results at larger adsorption percentage of 75%. The simulated adsorption time is longer than that from experiment at 75% percentage of

adsorption reflecting the relatively slower adsorption kinetics in the CO₂ breakthrough curves, as shown in Figure 25.

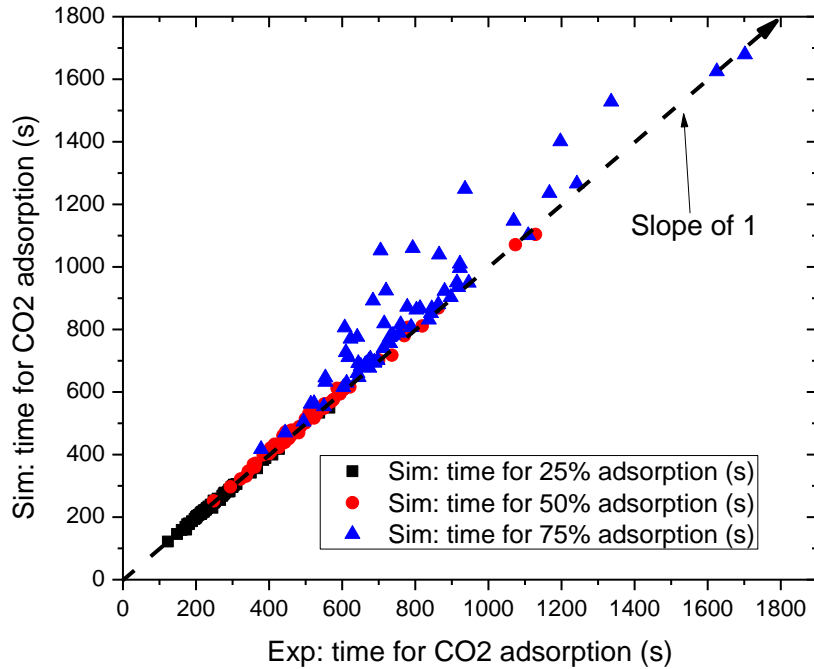


Figure 28 Experiment CO₂ adsorption time Vs. simulated adsorption time for 25%, 50% and 75% adsorption

7.2 UQ Analysis and Results for 32D Reacting Flow

The UQ analysis of the reacting flow is complicated by several factors: (i) There are three QOIs for each input setting (i.e., CO₂ adsorption, temperature, and pressure), and CO₂ adsorption is a functional breakthrough curve over time. (ii) The model has a total of 15 model parameters to calibrate, along with three inputs varying across the experiments. (iii) The CFD model runs are substantially more expensive now that the chemistry is coupled with the fluid dynamics. Ideally, the plan was to use the basic data calibration work from TGA data to both help specify prior distributions for the chemistry parameters and possibly eliminate some of those that did not have much influence (i.e., based on the posterior distribution resulting from that work). However, that work faced many complications, and those results were not available. Thus, we are faced with the far more difficult task here of calibrating the chemistry parameters from scratch.

With all of these complications, some simplification of the problem must first take place before the BSS-ANOVA calibration approach can be applied. To address complication (i) above, we decompose the functional breakthrough curves into a parametric form. Once the curves can be described in this manner, the coefficients representing the curves can become the outputs for calibration purposes. In order to be the most useful for calibration purposes, such a decomposition must be a parsimonious parameterization (i.e., leading to only a few outputs) that describes the shape of the curves in an interpretable manner. A conflicting goal

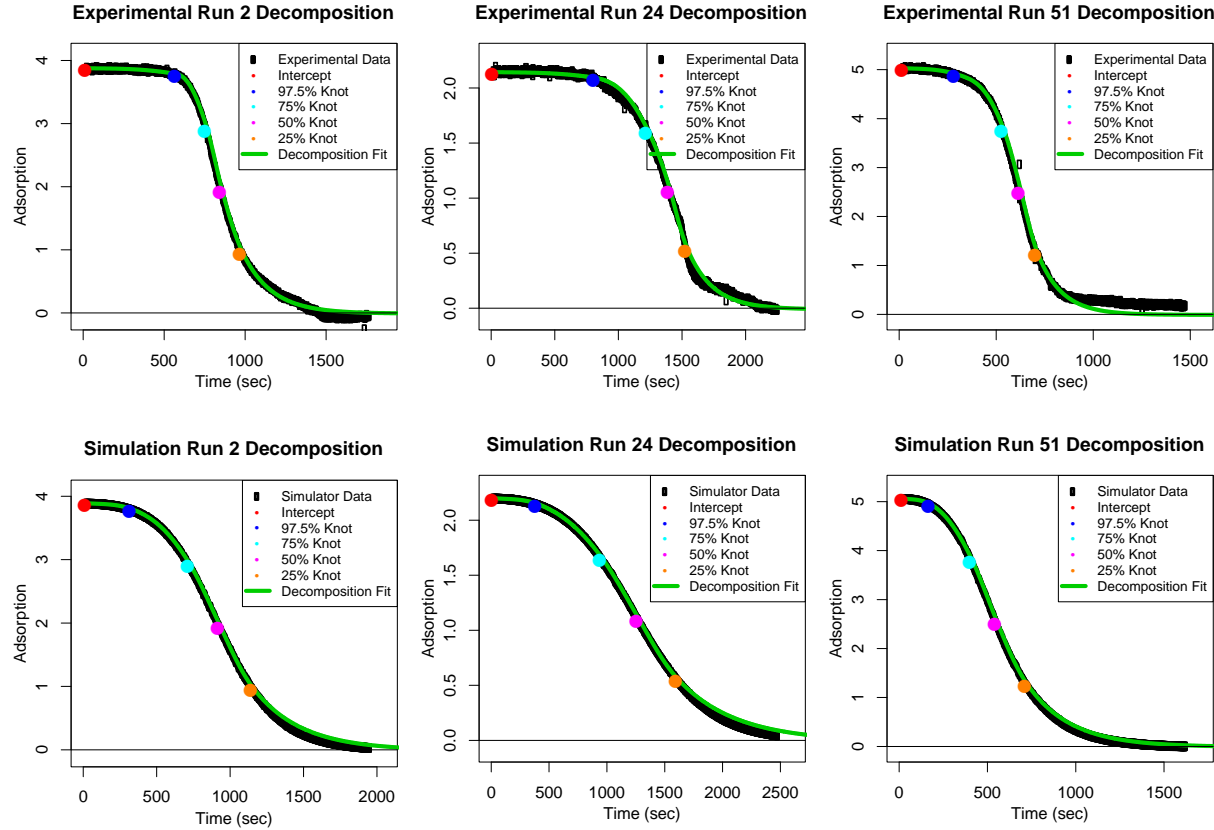


Figure 29 Functional decompositions for three of the experimental runs (top row) and three simulator runs at corresponding experimental input settings and the parameter settings used in Section 7.1.

is to also ensure that the parametric decomposition captures most of the variability in the curves (so that the model is calibrated to all relevant features)

Through some trial and error, a very accurate representation of the curves can be obtained by specifying the y -intercept (β_0), the time until the 2.5th, 25th, 50th, and 75th percent reductions from β_0 , (i.e., time elapsed until adsorption is $0.975\beta_0$, $0.75\beta_0$, $0.50\beta_0$, and $0.25\beta_0$), respectively, then interpolating these values with a monotone cubic log-spline. That is, the time until the respective percent reductions specifies the knot locations for the monotonic interpolating log-spline. A log-spline is simply a spline that is fit to the natural logarithm of the y values to ensure that the adsorption asymptotes out to zero. An interpolating spline can be restricted to be monotonic via the Hermite method (Burden & Faires, 2004). Several examples of this decomposition to experimental and simulated breakthrough curves are provided in Figure 29.

This approach also has the benefit of stabilizing the output from those experimental results that achieved steady state adsorption values significantly different from zero (e.g., Run 51 in the top right pane of Figure 29). Based on the replicate experimental runs, the measured adsorption for low values was far less repeatable, generally speaking, than for the higher levels. This seems likely due to measured adsorption being the difference between sensor readings for CO₂ concentration at the bottom and top of the adsorber, respectively, and expecting them to measure the same when there is *zero* adsorption, for example. Systematic measurement error for these sensors will convolve and lead to the greatest error for

measuring adsorption when CO₂ concentration and flow rate is high, but adsorption is low, i.e., the situation for the end of Run 51. In all likelihood the experimental data should be reading zero adsorption at the end of Run 51, but they are not. The decomposition curve, on the other hand, does assume it reaches zero adsorption in steady state.

Unlike the adsorption curves, the pressure drop PDT3820 and temperature output curves are well characterized by a simple average over the experiment. Thus, it would be sensible for the purpose of model calibration to the reacting data to use the outputs $y_1 = \beta_0$, $y_2 = t_{0.975}$, $y_3 = t_{0.75}$, $y_4 = t_{0.50}$, $y_5 = t_{0.25}$, $y_6 = \text{average PDT3820}$, $y_7 = \text{average Bed Temperature}$ (where t_q is the time until the curve reaches the value of $q\beta_0$). However, under this parameterization, it would be possible for the statistical BSS-ANOVA model to produce a value of $t_{0.75}$ that is greater than $t_{0.50}$, for example. While this is not likely, especially if there are enough simulator runs, it can lead to instability in the calibration procedure. The alternative parameterization of $y_1 = \beta_0$, $y_2 = \log(t_{0.975})$, $y_3 = \log(t_{0.75} - t_{0.975})$, $y_4 = \log(t_{0.50} - t_{0.75})$, $y_5 = \log(t_{0.25} - t_{0.50})$, $y_6 = \text{average PDT3820}$, $y_7 = \text{average Bed Temperature}$, allows the outputs to be unrestricted and hence does not suffer from this issue. Therefore this alternative parameterization is used to produce the results below.

The system inputs that were studied here along with their ranges are provided in Table 2. The model parameters that were included in the calibration along with their prior distributions are provided in Table 3. An LHS of size 52, with 19 points replicated (for a total of 71 points) was used to cover the experimental input space. Bivariate scatterplots of this design are displayed in Figure 30 Pairwise scatter plots of the space filling experimental design for C2U runs for adsorption. Replicated conditions are plotted in redFigure 30. The temperature that was used in the experimental design is the desired bed temperature. The coil temperature and gas inflow temperature are then automatically adjusted by the C2U to produce the desired bed temperature. However, the coil temperature and gas inflow temperature were then used as inputs to the MFIX model. C2U experiments were run at each of these 71 experimental settings and breakthrough curves, temperature and PDT3820 pressure differential were obtained.

Table 2 Experimental Inputs

Input	Range
x_1 = Gas inflow rate (slpm)	15.0 – 30.0
x_2 = partial pressure CO ₂ (%)	10.0 – 20.0
x_2 = Coil Temp (°C)	39.0 – 81.5
x_3 = Gas Inflow Temp (°C)	23.6 – 38.4

Table 3 Model Parameters and prior distributions

Parameter	Prior Distribution
$\theta_1 = \Delta H_x$	N(-78000, 11800^2) truncated over [-150000,-30000]
$\theta_2 = \Delta S_x$	N(-250, 25^2) truncated over [-320,-200]
$\theta_3 = \Delta H_x^{++}$	Uniform(30000, 120000)
$\theta_4 = \log_{10}(\zeta_x)$	Uniform(0, 5.5)
$\theta_5 = \Delta H_a$	Uniform(-100000, -10000)

$\theta_6 = \Delta S_a$	Uniform(-320, -200)
$\theta_7 = \Delta H_a^{++}$	Uniform(20000, 120000)
$\theta_8 = \log_{10}(\zeta_a)$	Uniform(0, 4)
$\theta_9 = \Delta H_b$	Uniform(-150000, -30000)
$\theta_{10} = \Delta S_b$	Uniform(-320, -200)
$\theta_{11} = \Delta H_b^{++}$	Uniform(25000, 120000)
$\theta_{12} = \log_{10}(\zeta_b)$	Uniform(0, 4)
θ_{13} = particle size (μm)	Beta(4.5, 3.3) shifted and scaled to [108,125]
θ_{14} = Effective amine % when fresh	N(0.177, 0.027 2) truncated over [0.133,0.210]
θ_{15} = Effective amine decay rate	N(0.0017, 0.00015 2) truncated over [0.0013,0.0022]

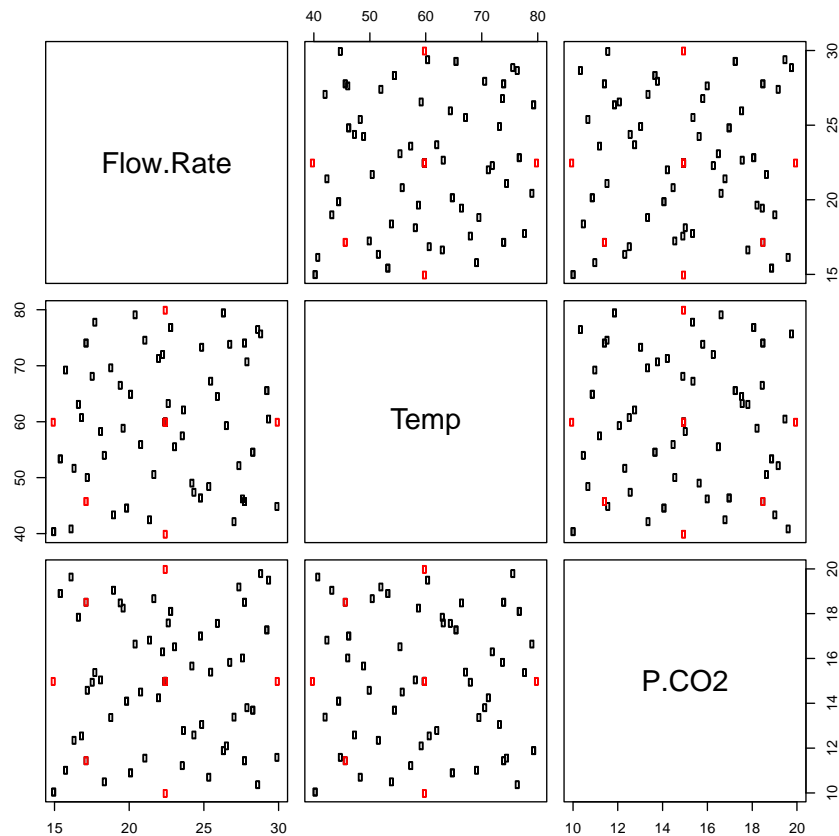


Figure 30 Pairwise scatter plots of the space filling experimental design for C2U runs for adsorption. Replicated conditions are plotted in red

An LHS sample of 100 runs (varying both the input settings uniformly on the ranges in Table 2 and model parameter settings according to their independent prior distributions in

Table 3) was generated and MFIX runs were made at these locations. Of these 100 runs, only 56 of them successfully completed. The failed runs were entirely due to the wide range of the parameter settings that had to be used for the chemistry model parameters (there were no failed MFIX runs in any previous studies). Thus, we augmented this initial LHS design with another 100 runs, of which 51 were successful.

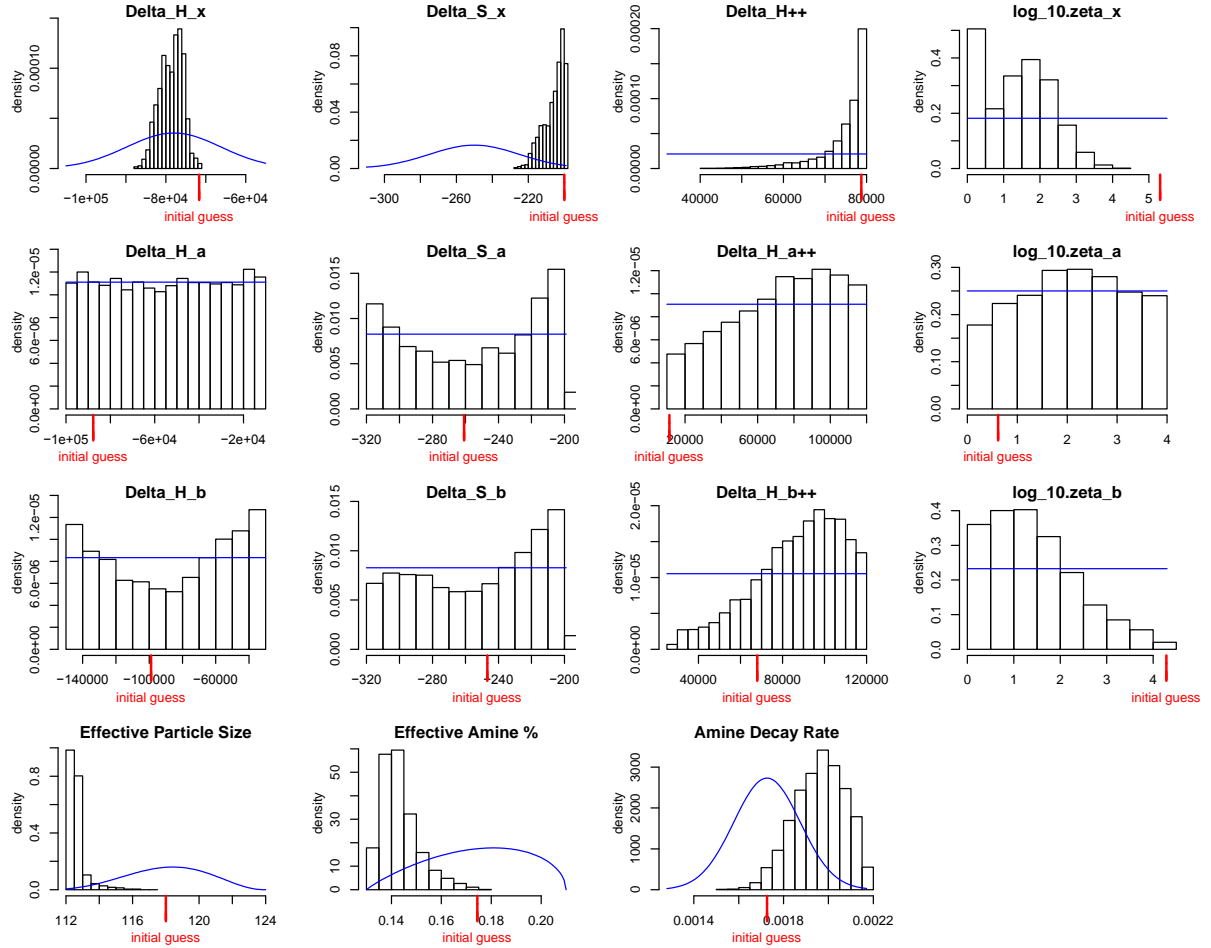


Figure 31Histograms of the marginal posterior distributions of the 15 model parameters. Prior density is given by the blue curve. The set points for the 71 MFIX validation runs described in Section 7.1 are given as the red ticks for reference

The total of the 107 successful runs from the LHS along with the 71 runs made at fixed parameter settings (as described in Section 7.1) were each processed into their respective values of y_1 through y_7 and used along with the same outputs from experimental observations in the BSS-ANOVA calibration tool. However, nine of the 71 experimental runs were held out from the analysis so that out-of-sample validation predictions can be made for these experimental settings without the benefit of their data influencing the calibration results. The nine holdout observations were chosen in such a manner that all of the corresponding replicated observations (if any) were held out as well. Histograms of the marginal posterior distributions of the 15 model parameters are provided in Figure 31 along with the respective prior distributions (blue curves).

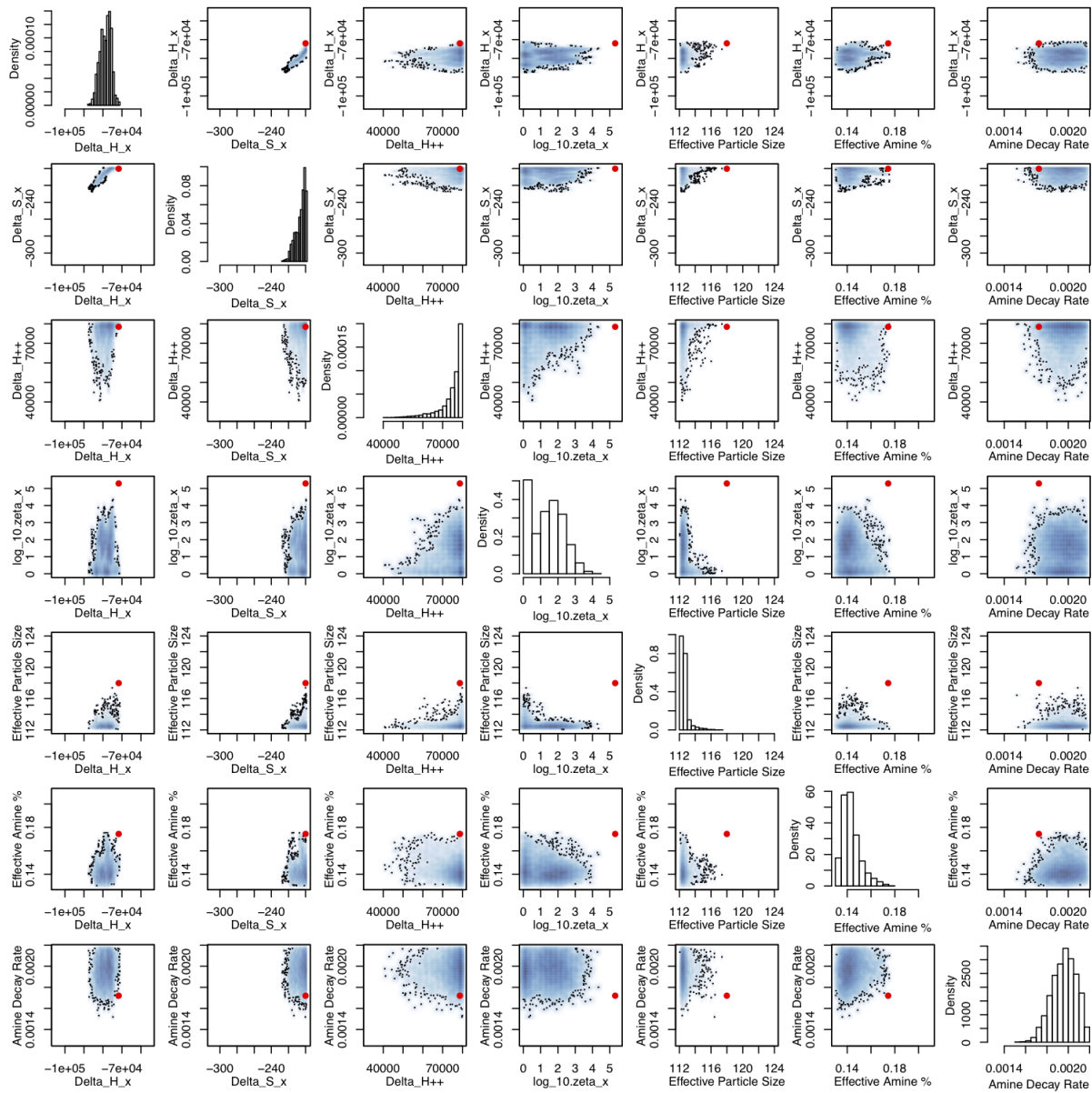


Figure 32 Bivariate view of the posterior distribution for all pairwise combinations of the seven influential model parameters. The univariate posterior distribution for a given parameter is provided along the diagonal.

The posterior distribution plotted along with the prior distribution serves a dual purpose

as a sensitivity analysis. For example, any parameter with a marginal posterior distribution substantially different from its prior has a substantial influence on one or more of the outputs. In this case it is clear that the first four parameters (i.e., chemistry parameters for dry reaction) have a substantial influence on the output. The 5th through 8th and 9th through 12th parameters that govern the physisorption and humid reactions respectively have very little influence on the output for this system. The model also shows some sensitivity to the effective particle size. Finally, the effective percentage of amine (for fresh sorbent) and the rate at which this is assumed to exponentially decay over time (in seconds) are also influential parameters. A more detailed sensitivity analysis (than the examination of the posterior distribution versus the prior) was conducted to examine the effect of each variable on each output (the numerous plots not shown). This determined that the outputs representing the decomposition of the breakthrough curve were sensitive primarily to the equilibrium parameters for dry reaction, ΔH_x and ΔS_x , and the effective amine percentage (and corresponding decay rate). Breakthrough curve is also sensitive, albeit to a much smaller extent, to the rate parameters for dry reaction ΔH_x^{++} and ζ_x . The pressure drop at PDT3820 was largely only affected by particle size.

The bivariate marginal posterior distributions are provided in Figure 32 as heat map plots for all pairwise combinations of the seven influential model parameters. The red points indicate the best available guess for the values of these parameters (as used in Section 7.1) prior to applying the calibration procedure. Posterior correlations between some parameters can be seen in this figure by observing the corresponding bivariate posterior cloud. If there is any kind of (nonzero slope) linear relation in a bivariate cloud, then there is some correlation. For example, ΔH_x and ΔS_x have a substantial amount of posterior correlation, as do ΔH_x^{++} and ζ_x .

Predictions of the breakthrough curves for the nine *held out* runs are provided in Figure 33. Prediction of a breakthrough curve is made by predicting y_1 through y_5 , then converting these “knot” predictions into a curve via the monotonic log-spline describe above. Many (~1000) predictions are obtained by sampling points from the posterior distribution (over the parameters, the emulator, and the discrepancy), then a posterior mean and 95% credible bands are obtained.

The emulator predictions are given as blue curves (mean and 95% credible bands). The posterior mean is the best guess prediction, while the bands include two forms of uncertainty (i) that due to the uncertainty in model parameters, and (ii) that due to the use of the emulator in place of the simulator. The discrepancy function is added to the emulator predictions to produce the emulator plus discrepancy predictions as red curves (mean and 95% credible bands). These bands are tighter than the simulator predictions alone, which is due more to emulator uncertainty than parameter uncertainty in this case. More simulator runs (particularly at these input/parameter locations) would reduce the width of these bands. This is being done in further work as a follow-on validation.

The raw experimental data is provided along with error bands (green) for the functional decomposition fit for the experimental observation. The green bands are representing the observation error with 95% confidence for what possible decomposition curve could be produced if the same experiment were repeated. The several replicate observations help

substantially with the stable estimation of this error covariance and production of such error bands. In actuality, there are not any *true* replicates in these experimental data because of the amine degradation effect. However, the replicated experimental conditions are still crucial to the identification of this degradation effect and the estimation of observation error in a complex calibration problem such as this.

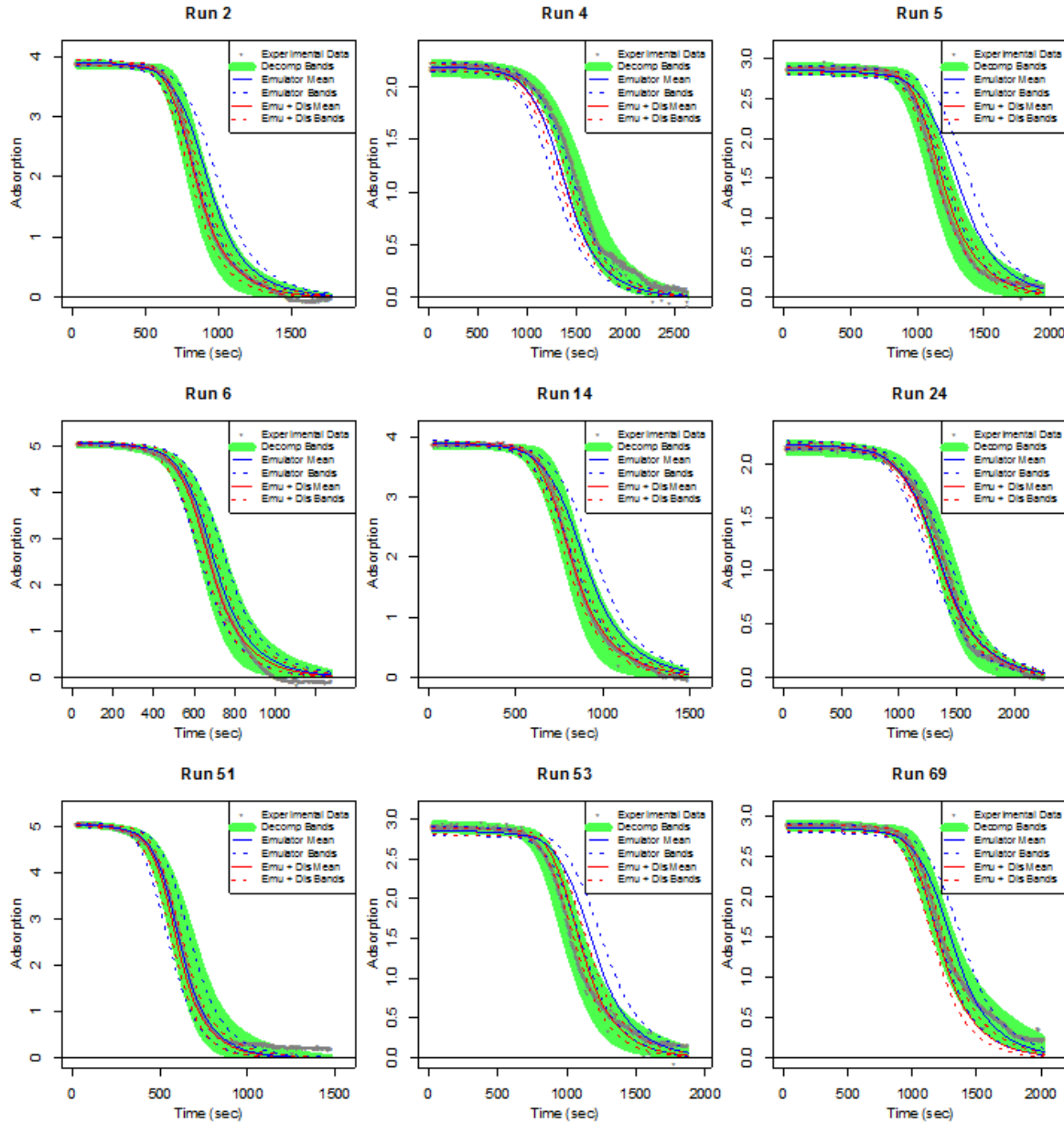


Figure 33 Predictions of the breakthrough curves for the nine held out runs along with experimental data (grey points) and experimental error bands based on the functional decomposition (green).

The discrepancy allows slightly more fidelity to the experimental observations, however, the emulator predictions are already very close to reality in all cases. The emulator

prediction bands are within observation error in all cases. Thus, there is no evidence that the model has a significant shortcoming on the basis of these predictions.

Figure 34 provides emulator posterior mean predictions versus the observed experimental observations for all 71 observations for all of the outputs y_1 through y_6 (y_7 , i.e., bed temperature, is not shown for ease of presentation since it was so easily predicted by the MFIX model as demonstrated in Section 7.1). The experimental observations are also provided for each case along with 95% error intervals (green). The predictions against the observed should, aside from error, fall on the $y = x$ line. If there were no model bias, there should be very few observations that do not have error intervals intersecting the $y = x$ line. Overall, the MFIX model (according to the emulator) is doing a very good job of predicting the experimental values as there are only a few observations that fall significantly (i.e., beyond observation error) off of the $y = x$ line.

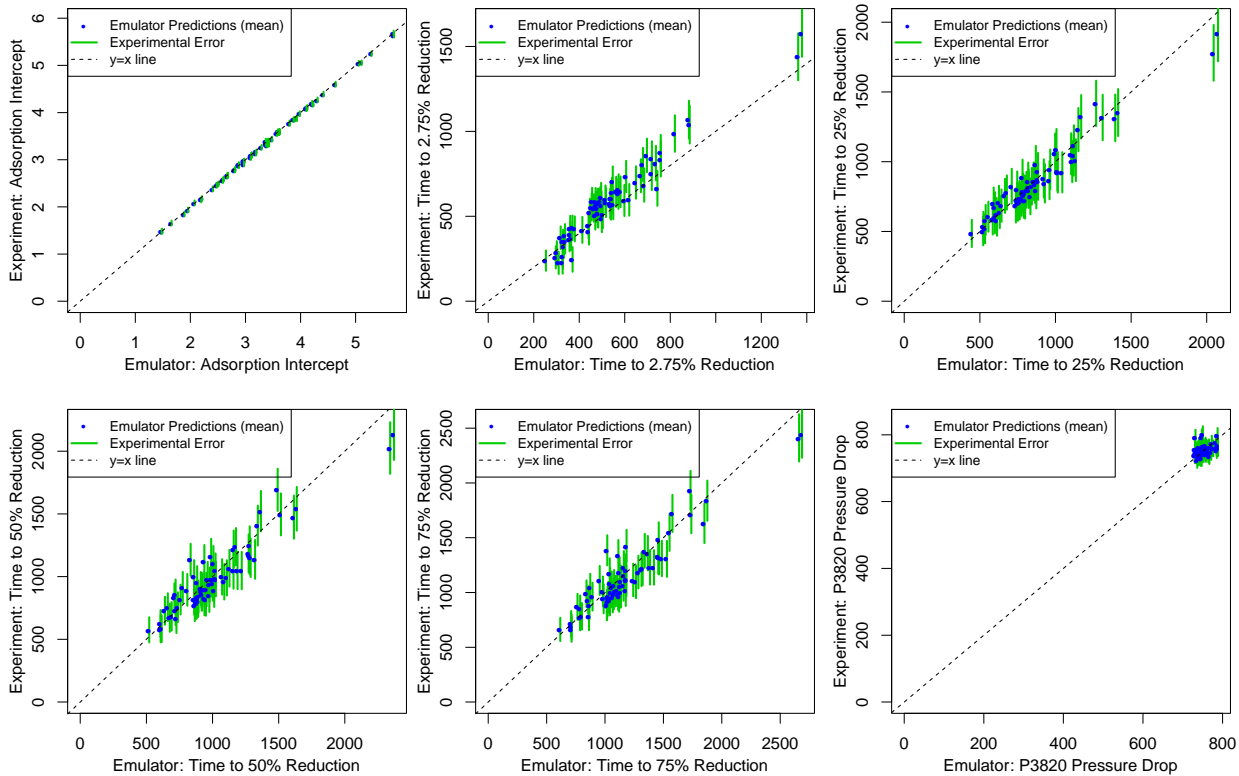


Figure 34 Emulator model predictions versus the observed data for the coefficients of the breakthrough curve decomposition along with predictions versus observed for the PDT3820 pressure drop.

Figure 34 provides the same predictions made in Figure 33 only the predictions include the model discrepancy term. Experimental observation error is represented with 2 times standard deviation green error bars. Emulator predictions are made using the posterior mean. Emulator uncertainty, which most certainly does exist as seen in Figure 33, is not represented in these plots. The predictions with model discrepancy are better, generally speaking, than the model predictions, which is typically the case. However, these predictions are not substantially better than the MFIX model alone for this system. Considering extrapolation

issues with the propagation of a model form discrepancy term for upscaling, it seems preferable in this case to use the model (or emulator) along with parameter uncertainty for predictions at scale.

Summary and Conclusions

The report summarized the detailed hierarchical model calibration and model validation procedures for predicting the device-scale CO₂ adsorption with a multi-phase reactive flow CFD model. Unit problems with increasing level of physical complexities are used as the building blocks for progressive model parameter calibration. Uncertainty quantification studies have been performed on various parameters that influence the behavior of the multi-phase flow hence the overall CO₂ adsorption of the reactor. Through this demonstration, a multi-phase reactive flow CFD model has been developed with the posterior model parameter distributions obtained through calibration with C2U experimental results as different unit problems. The ultimate goal of this work is to provide the CFD modeling methodology and the associated uncertainty quantification techniques that can be used in estimating the predictive confidence for the virtual scale up to a larger device.

Experiments and the corresponding modeling simulations have followed the hierarchical validation framework developed by the CCSI CFD team. Cold flow was studied first where only hydrodynamics is considered and pressure drop is the only QOI. Next, heat transfer is considered in 32D hot but non-reacting flow where bed temperature (temporal and spatial) is an added QOI. Finally, chemical reactions are introduced to the already complex coupled hydrodynamics and thermal transfer multi-phase flow problem, and CO₂ adsorption capacity and the breakthrough curve are added as additional QOIs. Overall, the CFD modeling results have demonstrated that MFIX multi-phase reactive flow models can be used to accurately capture the bed pressure, temperature and CO₂ capture capacity and kinetics of the C2U reactor.

In addition to the model parameters that are difficult to be quantified through experiments, sorbent particle size and twelve kinetics parameters that define the reaction rates and equilibrium status for three chemical reactions are also calibrated and found to be the most influential parameters. Through numerous simulations and calibrations, it is found that the effective particle size is higher than the nominal SMD in order to achieve better correlations of bed pressure and CO₂ adsorption breakthrough curve. By including the parameters from the first generation sorbent chemistry model in the CFD model calibration, posterior distributions have been derived to “match” the CO₂ adsorption breakthrough curve produced by the physical experiments (while accounting for uncertainty). In future study, we plan to calibrate the particle size to just pressure drop in the reacting case to verify the posterior distribution attained from this exercise is similar to that attained from the 32D cold flow and 32D hot, non-reacting cases. Finally, a more thorough sensitivity analysis of each model output will be conducted to assess how much influence on each output can be attributed to input parameters.

This hierarchical calibration and validation process has also demonstrated the importance of concurrence data exchange and knowledge flow in the multi-scale multi-physics

simulations: the discrepancy between the device-level measured and initial CFD predicted CO₂ adsorption kinetics with the original set of kinetics parameter provided by Task 2 has prompted the Task 2 team to further improve the parameter fit based on the TGA data from the fast reaction regime, the results of which in turn helped the Task 4 team in improving our overall predicted reactor-level CO₂ adsorption kinetics.

References

- Lane, W., Storlie, C., Montgomery, C. & Ryan, E. (2013), Numerical modeling and uncertainty quantification of a bubbling fluidized bed with immersed horizontal tubes, *Powder Technology* (in review).
- Saltelli, A., K., C. & Scott, E., eds (2000), *Sensitivity Analysis*, New York, NY: Wiley.
- CB Storlie, LP Swiler, JC Helton, and CJ Sallaberry (2009). Implementation and Evaluation of Nonparametric Regression Procedures for Sensitivity Analysis of Computationally Demanding Models. *Reliability Engineering and System Safety* 94 (11), 1735-1763.
- M. C. Kennedy, A. O'Hagan, Bayesian Calibration of Computer Models, *Journal of the Royal Statistical Society B* 63 (2001) 425–464.
- D. Higdon, M. Kennedy, J. Cavendish, Combining field data and computer simulations for calibration and prediction, *SIAM Journal on Scientific Computing* (26) (2004) 448–466.
- CB Storlie, WA Lane, EM Ryan (2013). Calibration of Computational Models with Categorical Parameters and Correlated Outputs via Bayesian Smoothing Spline ANOVA. *Journal of the American Statistical Association* (in review).
- J. Helton, F. Davis, Latin hypercube sampling and the propagation of uncertainty in analyses of complex systems, *Reliability Engineering & System Safety* 81 (1) (2003) 23–69.
- T. Trevor, “Influence of Particle Size Distribution on Fluidized Bed Hydrodynamics”, The University of Western Ontario.
- Wen, C.Y. Wen and Y.H. Yu, (1966), A generalized method for predicting the minimum fluidization velocity. *AIChE J.*, 12: 610–612. doi: 10.1002/aic.690120343
- H. Krutka, S. Sjostrom, Evaluation of Solid Sorbents as a Retrofit Technology for CO₂ Capture from Coal-fired Power Plants, Final Technical Report, DOE Award Number DE-NT0005649, Report Number 05649FR01.
- Y. Igci, A.T. Andrews, S. Sundaresan, S. Pannala, T. O'Brien, 2008. Filtered two-fluid models for fluidized gas-particle suspensions. *AIChE Journal* 54, 1431-1448.
- Y. Igci, S. Sundaresan, 2011. Constitutive Models for Filtered Two-Fluid Models of Fluidized Gas–Particle Flows. *Industrial & Engineering Chemistry Research* 50, 13190-13201.

Milioli C.C., Milioli F.E., Holloway W., Agrawal K. and Sundaresan S., Filtered Two-Fluid Models of Fluidized Gas-Particle Flows: New Constitutive Relations. *AIChE Journal*, 59: 3265–3275, 2013. doi: 10.1002/aic.14130.

E.R. Monazam, L.J. Shadle, D.C. Miller, H.W. Pennline, D.J. Fauth, J.S. Hoffman, M.L. Gray (2013) Equilibrium and Kinetics Analysis of Carbon Dioxide Capture using Immobilized Amine on a Mesoporous Silica” *AIChE Journal*, 59 (3) 923-935.

D. Mebane, D. Fauth, A. Lee, *First Generation Model for Silica-Supported Amine Sorbent NETL 32D*, NETL Report for Carbon Capture Simulation Initiative, July 2012.

Burden R.L., Faires, J.D. (2004). *Numerical Analysis*. Belmont: Brooks/Cole.